APPENDIX C

ENVIRONMENTAL FLUID DYNAMICS CODE (EFDC) MODEL

APPENDIX C.1

THE ENVIRONMENTAL FLUID DYNAMICS CODE (EFDC): HYDRODYNAMIC THEORETICAL AND TECHNICAL ASPECTS

TABLE OF CONTENTS

Appendix C.1

Environmental Fluid Dynamics Code (EFDC): Hydrodynamic Theoretical and Technical Aspects

MODEL DESCRIPTION

Introduction

The environmental fluid dynamics code (EFDC) is a general-purpose modeling package for simulating three-dimensional (3-D) flow, transport, and biogeochemical processes in surface water systems including: rivers, lakes, estuaries, reservoirs, wetlands, and near-shore to shelf-scale coastal regions. The EFDC model was originally developed at the Virginia Institute of Marine Science for estuarine and coastal applications and is considered public domain software. In addition to hydrodynamic and salinity and temperature transport simulation capabilities, EFDC is capable of simulating cohesive and noncohesive sediment transport, near-field and far-field discharge dilution from multiple sources, eutrophication processes, the transport and fate of toxic contaminants in the water and sediment phases, and the transport and fate of various life stages of fish and shellfish. Special enhancements to the hydrodynamic portion of the code, including vegetation resistance, drying and wetting, hydraulic structure representation, wave-current boundary layer interaction, and wave-induced currents, allow refined modeling of wetland and marsh systems, controlled-flow systems, and near-shore wave-induced currents and sediment transport. The EFDC code has been extensively tested and documented and used in more than 20 modeling studies. The code is currently used by university, government, and engineering and environmental consulting organizations. The following sections summarize the major features and capabilities of the EFDC modeling package that will be used in the Housatonic River modeling project.

Hydrodynamics

The physics of the EFDC model and many aspects of the computational scheme are equivalent to the widely used Blumberg-Mellor model (Blumberg and Mellor, 1987) and the U.S. Army Corps of Engineers CH3D or Chesapeake Bay model (Johnson et al., 1993). The EFDC model solves the vertically hydrostatic, free-surface, turbulent-averaged equations of motions for a variable-density fluid. Dynamically coupled transport equations for turbulent kinetic energy, turbulent length scale, salinity, and temperature are also solved. The two turbulence parameter transport equations implement the Mellor-Yamada level 2.5 turbulence closure scheme (Mellor and Yamada, 1982; Galperin et al., 1988). The EFDC model uses a stretched or sigma vertical coordinate and cartesian or curvilinear, orthogonal horizontal coordinates.

The numerical scheme used in EFDC to solve the equations of motion uses second-order accurate spatial finite differencing on a staggered or C grid. The model's time integration uses a second-order accurate three time-level, finite difference scheme with a internal-external mode splitting procedure to separate the internal shear or baroclinic mode from the external free-surface gravity wave or barotropic mode. The external mode solution is semi-implicit, and simultaneously computes the two-dimensional surface elevation field by a preconditioned

conjugate gradient procedure. The external solution is completed by the calculation of the depth-averaged barotropic velocities using the new surface elevation field. The model's semi-implicit external solution allows large time steps that are constrained only by the stability criteria of the explicit central difference or high-order upwind advection scheme (Smolarkiewicz and Margolin, 1993) used for the nonlinear accelerations. Horizontal boundary conditions for the external mode solution include options for simultaneously specifying the surface elevation only, the characteristic of an incoming wave (Bennett and McIntosh, 1982), free radiation of an outgoing wave (Bennett, 1976; Blumberg and Kantha, 1985), or the normal volumetric flux on arbitrary portions of the boundary. The EFDC model's internal momentum equation solution, at the same time step as the external, is implicit with respect to vertical diffusion. The internal solution of the momentum equations is in terms of the vertical profile of shear stress and velocity shear, which results in the simplest and most accurate form of the baroclinic pressure gradients and eliminates the over-determined character of alternate internal mode formulations. Time splitting inherent in the three time-level scheme is controlled by periodic insertion of a second-order accurate two-time level trapezoidal step. The EFDC model is also readily configured as a two-dimensional model in either the horizontal or vertical planes.

The EFDC model implements a second-order accurate in space and time, mass conservation fractional-step solution scheme for the Eulerian transport equations for salinity, temperature, suspended sediment, water quality constituents, and toxic contaminants. The transport equations are temporally integrated at the same time step or twice the time step of the momentum equation solution (Smolarkiewicz and Margolin, 1993). The advective step of the transport solution uses either the central difference scheme used in the Blumberg-Mellor model or a hierarchy of positive definite upwind difference schemes. The highest accuracy upwind scheme, second-order accurate in space and time, is based on a flux-corrected transport version of Smolarkiewicz's multidimensional positive definite advection transport algorithm (Smolarkiewicz and Clark, 1986; Smolarkiewicz and Grabowski, 1990), which is monotonic and minimizes numerical diffusion. The horizontal diffusion step, if required, is explicit in time, while the vertical diffusion step is implicit. Horizontal boundary conditions include time variable material inflow concentrations, upwinded outflow, and a damping relaxation specification of climatological boundary concentration. For the temperature transport equation, the NOAA Geophysical Fluid Dynamics Laboratory's atmospheric heat exchange model (Rosati and Miyakoda, 1988) is implemented.

Sediment Transport

The EFDC code is capable of simulating the transport and fate of multiple size classes of cohesive and noncohesive suspended sediment, including bed deposition and resuspension. Water column transport is based on the same high-order advection-diffusion scheme used for salinity and temperature. A number of options are included for the specification of settling velocities. For the transport of multiple size classes of cohesive sediment, an optional flocculation model (Burban et al., 1989 and 1990) can be activated. Sediment mass conservative deposited bed formulations are included for both cohesive and noncohesive sediment. The deposited bed may be represented by a single layer or multiple layers. The multiple-bed layer option provides a time-since-deposition versus vertical position in the bed relationship to be established. Water column-sediment bed interface elevation changes can be optionally

incorporated into the hydrodynamic continuity equation. An optional, one-dimensional in the vertical, bed-consolidation calculation can be performed for cohesive beds.

Toxic Contaminant Transport and Fate

The EFDC code includes two internal submodels for simulating the transport and fate of toxic contaminants. A simple, single-contaminant submodel can be activated from the master input file. The simple model accounts for water and suspended sediment phase transport with equilibrium partitioning and a lumped first-order reaction. Contaminant mass per unit area in the sediment bed is also simulated. The second, more complex submodel simulates the transport and fate of an arbitrary number of reacting contaminants in the water and sediment phases of both the water column and sediment bed. In this mode, the contaminant transport and fate simulation is functionally similar to the WASP5 TOXIC model (Ambrose et al., 1993) with the added flexibility of simulating an arbitrary number of contaminants, and the improved accuracy of more complex three-dimensional physical transport fields in a highly accurate numerical-transport scheme. Water-sediment phase interaction may be represented by equilibrium or nonlinear sorption processes. In this mode, the multilayer sediment bed formulation is active, with sediment bed water volume and dissolved contaminant mass balances activated to allow contaminants to reenter the water column by both sediment resuspension, pore water expulsion due to consolidation, and diffusion from the pore water into the water column. The complex contaminant model activates a subroutine describing reaction processes with appropriate reaction parameters provided by a toxic reaction processes input file.

Wetland, Marsh, and Tidal Flat Simulation Extension

The EFDC model provides a number of enhancements for the simulation of flow and transport in wetlands, marshes, and tidal flats. The code allows for drying and wetting in shallow areas by a mass-conservative scheme. This capability will be used to simulate periodic overbank flood flow onto the floodplain of the Housatonic River. The drying and wetting formulation is coupled to the mass transport equations in a manner that prevents negative concentrations of dissolved and suspended materials. A number of alternatives are in place in the model to simulate general discharge control structures such as weirs, spillways, culverts, and water surface elevation-activated pumps. The effect of submerged and emergent plants is incorporated into the turbulence-closure model and flow-resistance formulation. Plant density and geometric characteristics of individual and composite plants are required as input for the vegetation-resistance formulation. A simple soil moisture model, allowing rainfall infiltration and soil water loss due to evapotranspiration under dry conditions, is implemented.

To represent narrow channels and canals in wetland, marsh, and tidal flat systems, a subgrid scale channel model is implemented. The subgrid channel model allows a network of one-dimensional (1-D) in the horizontal channels to be dynamically coupled to the two-dimensional (2-D) in the horizontal grid representing the wetland, marsh, or tidal flat system. Volume and mass exchanges between 2-D wetland cells and the 1-D channels are accounted for. The channels may continue to flow when the 2-D wetland cells become dry. Although not explicitly designed for application to riverine floodplains, the subgrid scale channel capability of EFDC will be tested as a feasible strategy to couple coarse cartesian floodplain grid cells with the narrow Housatonic River channel.

Near-shore Wave-Induced Currents and Sediment Transport Extensions

The EFDC code includes a number of extensions for simulation of near-shore wave-induced current and noncohesive sediment transport. The extensions include a wave-current boundary layer formulation similar to that of Grant and Madsen (1986); modifications of the hydrodynamic model's momentum equations to represent wave period-averaged Eulerian mean quantities; the inclusion of 3-D wave-induced radiation or Reynold's stresses in the momentum equations; and modifications of the velocity fields in the transport equations to include advective transport by the wave-induced Stoke's drift. High-frequency surface wave fields are provided by an external wave refraction-diffraction model or by an internal mild slope equation submodel similar to that of Madsen and Larsen (1987). The internal refraction-diffraction computation is executed on a refined horizontal grid coincident with the main model's horizontal grid.

User Interface

The EFDC modeling package's user interface is based on text input file templates. This choice was selected in the interest of maintaining model portability across a range of computing platforms and readily allows the model user to modify input files using most text-editing software. The text interface also allows modification of model files on remote computing systems and in heterogeneous network environments. All input files have standard templates available with the EFDC code and in the digital version of the user's manual. The file templates include extensive built-in documentation and explanation of numerical input data quantities. Actual numerical input data are inserted into the text template in a flexible free format as internally specified in the file templates. Extensive checking of input files is implemented in the code and diagnostic on-screen messages indicate the location and nature of input file errors. All input files involving dimensional data have unit conversion specifications for the MKS unit system used internally in the model.

Preprocessing Software

The EFDC modeling package includes a grid-generating preprocessor code, GEFDC, which is used to construct the horizontal model grid, interpolate bathymetry, and initial fields such as water surface elevation and salinity, to the grids. EFDC input files specifying the grid geometry and initial fields are generated by the preprocessor. The preprocessor is capable of generating Cartesian and curvilinear-orthogonal grids using a number of grid-generation schemes (Mobley and Stewart, 1980; Ryskin and Leal, 1983; Kang and Leal, 1992).

Model Configuration

The EFDC code exists in only one generic version. A model application is specified entirely by information in the input files. To minimize memory requirements for specific applications, an executable file for the application is created by setting appropriate model variable array sizes in the model's parameter file and compiling the source code. The EFDC model may be configured to execute all or a portion of a model application in reduced-spatial-dimension mode, including 2-D depth or width-averaged and 1-D cross section averaged. The number of layers used in the 3-D mode or 2-D width-averaged mode is readily changed by one line of model input. Model grid sections specified as 2-D width averaged are allowed to have depth-varying widths to

provide representations equivalent to those of 2-D width-averaged estuarine and reservoir models such as CE- QUAL-W2 (Cole and Buchak, 1994).

Run Time Diagnostics

The EFDC modeling package includes extensive built-in run time diagnostics that may be activated in the master input file by the model user. Representative diagnostics include records of maximum CFL numbers, times and locations of negative depths, a variety of volume and mass balance checks, and global mass and energy balances. An on-screen print of model variables in a specified cell can be activated during modeling execution. A number of log files are generated during model execution that allow additional diagnostics of run time problems encountered in setting up a new application.

Model Output Options

A wide variety of model output options are available. These options include specification of output files for horizontal plane and vertical plane transect plotting of vector and scalar field at specified time; the generation of time series of model variables at selected locations and time intervals; grab sample simulation at specified times and locations; and the specification of least-squares analysis of selected model variables at a defined location over a specified interval. A general 3-D output option allows output of all major model variables in a compressed form at specified times. A restart file is generated at user-specified intervals during model execution.

Postprocessing, Graphics, and Visualization

The generic model output files may be readily processed by a number of third-party graphics and visualization software packages, often without need for intermediate processing (Rennie and Hamrick, 1992). The availability of the source code to the user allows the code to be modified for specific output options. Graphics and visualization software successfully used with EFDC output include APE, AVS, IDL, Mathematica, MatLab, NCAR Graphics, PV-Wave, Techplot, SiteView, Spyglass Transform and Slicer, and Voxelview. The model developer currently uses Spyglass and Voxelview and a number of special image enhancement postprocessor applications are available for these products.

Documentation

Extensive documentation of the EFDC model is available. Theoretical and computational aspects of the model are described for hydrodynamics (Hamrick, 1992a), sediment transport (Tetra Tech, 2000), and toxic contaminants (Tetra Tech, 1999). The model user's manual (Hamrick, 1996) provides details on use of the GEFDC preprocessor and setup of the EFDC input files. Input file templates are also included. A number of papers (Hamrick, 1992b; Hamrick, 1994; Moustafa and Hamrick, 1994; Hamrick and Wu, 1997; and Wu et al., 1997) describe model applications and capabilities.

Computer Requirements

The EFDC modeling system is written in FORTRAN 77. The few nonstandard VAX FORTRAN language extensions in the code are supported by a wide variety of ANSI standard

FORTRAN 77 compilers. The generic or universal source code has been compiled and executed on most UNIX workstations (DEC Alpha, Hewlett-Packard, IBM RISC6000, Silicon Graphics, Sun and Sparc compatibles), Cray and Convex supercomputers, and PC compatibles and Macintosh personal computers. Absoft, Lahey, and Microsoft compilers are supported on PC compatibles, while Absoft, Language Systems, and Motorola compilers are supported on Macintosh and compatible systems.

Availability

The EFDC source code, file templates, preprocessing and postprocessing software, and user's manual are available from the code's principal developer, John M. Hamrick (email: ham@visi.net). An earlier version of the code is available from the Virginia Institute of Marine Science in the HEM3D (Hydrodynamic-Eutrophication Model: 3D) modeling package.

References

Ambrose, R.B., T.A. Wool, and J.L. Martin, 1993: The water quality analysis and simulation program, WASP5: Part A, model documentation version 5.1. U.S. EPA, Athens Environmental Research Laboratory, 210 pp.

Bennett, A. F., 1976: Open boundary conditions for dispersive waves. *J. Atmos. Sci.,* 32, 176-182.

Bennett, A.F., and P.C. McIntosh, 1982: Open ocean modeling as an inverse problem: tidal theory. *J. Phys. Ocean.,* 12, 1004-1018.

Blumberg, A.F., and L.H. Kantha, 1985: Open boundary condition for circulation models. *J. Hydr. Engr.,* 111, 237-255.

Blumberg, A.F., and G.L. Mellor, 1987: A description of a three-dimensional coastal ocean circulation model. In: Three-Dimensional Coastal Ocean Models, Coastal and Estuarine Science, Vol. 4. (Heaps, N. S., ed.) American Geophysical Union, pp. 1-19.

Burban, P.Y., W. Lick, and J. Lick, 1989: The flocculation of fine-grained sediments in estuarine waters. *J. Geophys.* Res., 94, 8323-8330.

Burban, P.Y., Y. J. Xu, J. McNeil, and W. Lick, 1990: Settling speeds of flocs in fresh and seawater. *J. Geophys. Res.,* 95, 18,213-18,220.

Cole, T.M., and E.M. Buchak, 1994: CE-QUAL-W2: A two-dimensional laterally averaged, hydrodynamic and water quality model, Version 2.0. U. S. Army Corps of Engineers, Waterway Experiment Station, Vicksburg, MS, Report ITL-93-7.

Galperin, B., L.H. Kantha, S. Hassid, and A. Rosati, 1988: A quasi-equilibrium turbulent energy model for geophysical flows. *J. Atmos. Sci.,* 45, 55-62.

Grant, W.D., and O.S. Madsen, 1986: The continental-shelf bottom boundary layer. In: Annual Review of Fluid Mechanics, (Van Dyke, M. et al., eds.) Annual Review, Inc., pp. 365-306.

Hamrick, J.M., 1992a: A Three-Dimensional Environmental Fluid Dynamics Computer Code: Theoretical and Computational Aspects. The College of William and Mary, Virginia Institute of Marine Science. Special Report 317, 63 pp.

Hamrick, J.M., 1992b: Estuarine environmental impact assessment using a three-dimensional circulation and transport model. Estuarine and Coastal Modeling, Proceedings of the 2nd International Conference, M. L. Spaulding et al., Eds., American Society of Civil Engineers, New York, 292-303.

Hamrick, J.M., 1994: Linking hydrodynamic and biogeochemical transport models for estuarine and coastal waters. Estuarine and Coastal Modeling, Proceedings of the 3nd International Conference, M. L. Spaulding et al., Eds., American Society of Civil Engineers, New York, 591-608.

Hamrick, J.M., 1996: A User's Manual for the Environmental Fluid Dynamics Computer Code (EFDC). The College of William and Mary, Virginia Institute of Marine Science, Special Report 331, 234 pp.

Hamrick, J.M., and T.S. Wu, 1997: Computational design and optimization of the EFDC/HEM3D surface water hydrodynamic and eutrophication models. Chapter 16 In: Next Generation Environmental Models and Computational Methods, G. Delic and M.F. Wheeler, Eds., Society of Industrial and Applied Mathematics, Philadelphia.

Johnson, B.H., K.W. Kim, R.E. Heath, B.B. Hsieh, and H.L. Butler, 1993: Validation of three-dimensional hydrodynamic model of Chesapeake Bay. *J. Hyd. Engrg.*, 119, 2-20.

Kang, I.S., and L.G. Leal, 1992: Orthogonal grid generation in a 2D domain via the boundary integral technique. *J. Comp. Phys.*, 102, 78-87.

Madsen, P.A., and J. Larsen, 1987: An efficient finite-difference approach to the mild-slope equation. Coastal Engr., 11, 329-351.

Mellor, G.L., and T. Yamada, 1982: Development of a turbulence closure model for geophysical fluid problems. Rev. Geophys. Space Phys., 20, 851-875.

Mobley, C.D., and R.J. Stewart, 1980: On the numerical generation of boundary-fitted orthogonal Curvilinear coordinate systems. *J. Comp. Phys.*, 34, 124-135.

Moustafa, M.Z., and J.M. Hamrick, 1994: Modeling circulation and salinity transport in the Indian River Lagoon. Estuarine and Coastal Modeling, Proceedings of the 3nd International Conference, M. L. Spaulding et al., Eds., American Society of Civil Engineers, New York, 381-395.

Rennie, S., and J.M. Hamrick, 1992: Techniques for visualization of estuarine and coastal flow fields. Estuarine and Coastal Modeling, Proceedings of the 2nd International Conference, M. L. Spaulding et al., Eds., American Society of Civil Engineers, New York, 48-55.

Rosati, A.K., and K. Miyakoda, 1988: A general circulation model for upper ocean simulation. *J. Phys. Ocean.,* 18, 1601-1626.

Ryskin, G. and L.G. Leal, 1983: Orthogonal mapping. *J. Comp. Phys.,* 50, 71-100.

Smolarkiewicz, P.K., and T.L. Clark, 1986: The multidimensional positive definite advection transport algorithm: further development and applications. *J. Comp. Phys.,* 67, 396-438.

Smolarkiewicz, P.K., and W.W. Grabowski, 1990: The multidimensional positive definite advection transport algorithm: nonoscillatory option. *J. Comp. Phys.,* 86, 355-375.

Smolarkiewicz, P.K., and L.G. Margolin, 1993: On forward-in-time differencing for fluids: extension to a curvilinear framework. Mon. Weather Rev., 121, 1847-1859.

Tetra Tech, Inc., 2000: A theoretical description of sediment transport formulations used in the EFDC model. Tech. Memo TT-EFDC-00-1, Tetra Tech, Inc., Fairfax, VA.

Tetra Tech, Inc., 1999: A theoretical description of toxic contaminant transport formulations used in the EFDC model. Tech. Memo TT-EFDC-99-2, Tetra Tech, Inc., Fairfax, VA.

Wu, T.S., J.M. Hamrick, S.C. McCutcheon, and R.B. Ambrose, 1997. Benchmarking the EFDC/HEM3D surface water hydrodynamic and eutrophication models. Next Generation Environmental Models and Computational Methods, G. Delic and M.F. Wheeler, Eds., Society of Industrial and Applied Mathematics, Philadelphia.

APPENDIX C.2

EFDC PARAMETER LIST

Housatonic River EFDC Model Parameters

	Definition/Description	Units	Data Source
Volumetric Source/Sinks			
Upstream Boundary Conditions			
QSER	Volumetric inflow time series for East and West Branches of the Housatonic River	(m^3/s)	HSPF
CSER(,,,1)	Salinity Time Series (not used)	(ppt)	NA
CSER(,,,2)	Temperature Time Series	(°C)	HSPF
Cohesive Seds (CSER)	Cohesive Time Series (One for each class)	(g/m^3)	HSPF
NonCohesive Seds (CSER)	NonCohesive Series	(g/m^3)	HSPF
Toxics (CSER)	Toxic Time Series	(g/m^3)	Derived
Point Source Tributary			
QSER	Volumetric inflow time series for each tributary	(m^3/s)	HSPF
CSER(,,,1)	Salinity Time Series (not used)	(ppt)	NA
CSER(,,,2)	Temperature Time Series	(°C)	HSPF
Cohesive Seds (CSER)	Cohesive Time Series (One for each class)	(g/m^3)	HSPF
NonCohesive Seds (CSER)	NonCohesive Series	(g/m^3)	HSPF
Toxics (CSER)	Toxic Time Series	(g/m^3)	HSPF
External Point Source Loadings			
QSER	Volumetric inflow time series for each tributary	(m^3/s)	Site
CSER(,,,1)	Salinity Time Series (not used)	(ppt)	NA
CSER(,,,2)	Temperature Time Series	(°C)	Site
Cohesive Seds (CSER)	Cohesive Time Series (One for each class)	(g/m^3)	Site
NonCohesive Seds (CSER)	NonCohesive Series	(g/m^3)	Site
Toxics (CSER)	Toxic Time Series	(g/m^3)	Site
Non-Point Source (Distributed)			
QSER	Volumetric inflow time series for each tributary	(m^3/s)	HSPF
CSER(,,,1)	Salinity Time Series (not used)	(ppt)	NA
CSER(,,,2)	Temperature Time Series	(°C)	HSPF
Cohesive Seds (CSER)	Cohesive Time Series (One for each class)	(g/m^3)	HSPF
NonCohesive Seds (CSER)	NonCohesive Series	(g/m^3)	HSPF
Toxics (CSER)	Toxic Time Series	(g/m^3)	HSPF
Constant Source/Sinks	(Not used for the Housatonic)		
Flow/Temp/Toxic/Seds	A contant value for each parameter for the entire simulation		NA
Setup/Settings/Assumptions			
NTOX	# of toxic contaminants		Lit/Site
NSED	# of cohesive sediment size classes		Lit/Site
NSND	# of non-cohesive sediment size classes		Lit/Site
Cohesive Settings	Needed nsed times		
SDEN	Sediment specific volume	(m^3/g)	Site
SSG	Sediment specific gravity		Lit/Site
WSEDO	Constant or reference sediment settling velocity	(m/s)	Lit/Site
SEDSN	Normalizing sediment concentration	(g/m^3)	Lit/Site
TAUD	Boundary stress below which deposition takes place	(m^2/s^2)	Lit/Site
IWRSP	0 - Use specified resuspension rate and critical stresses >1 - Use bed properties dependent (computed) resuspension rate and critical stresses		Lit/Site
WRSPO	Reference surface erosion rate	(g/m^2-s)	Lit/Site
TAUR	Boundary stress above which surface erosion occurs	(m^2/s^2)	Lit/Site
TAUN	Normalizing stress	(m^2/s^2)	Lit/Site
TEXP	Exponent for surface erosion		Lit/Site
NonCohesive Settings	Needed nsnd times		
SDEN	Sediment spec volume (ie 1/2.65e6 m**3/gm)	(m^3/g)	Lit/Site
SSG	Sediment specific gravity		Lit/Site
SNDDIA	Representative diameter of sediment class	(m)	Lit/Site
WSNDO	Constant or reference sediment settling velocity	(m/s)	Lit/Site
SNDN	Maximum mass/Total volume in bed	(g/m^3)	3
TAUD	Dune break point stress	(m^2/s^2)	Lit/Site
ISNDEQ:	>1 Calculate above bed reference nonchohesive sediment equilibrium concentration 1 - Garcia and Parker, 2 - Smith and McLean, 3 - van Rijn		Lit/Site
TAUR	Critical Shields stress (water density normalized)	(m^2/s^2)	Lit/Site
TAUN	Normalizing stress	(m^2/s^2)	Lit/Site
TEXP	Critical Shields parameter		Lit/Site

Housatonic River EFDC Model Parameters

	Definition/Description	Units	Data Source
Volumetric Source/Sinks			
Toxic Settings	Needed for each nsed and nsnd		
NTOXC	Toxic contaminant number ID.		
ITXPARW	Flag to enable solids dependent partitioning in the water column		Lit/Site
TOXPARW	Water column partitioning coefficient between each toxic and sediment class	(l/mg)	Lit/Site
CONPARW	Exponent in Water column solids dependent partitioning		Lit/Site
ITXPARB	Flag to enable solids dependent partitioning in the bed		Lit/Site
TOXPARB	Sediment bed partitioning coefficient between each toxic and sediment class	(l/mg)	Lit/Site
CONPARB	Exponent in sediment solids dependent partitioning		Lit/Site
RKTOXW	First order water column decay rate for toxic variable	(s^{-1})	Lit/Site
TKTOXW	Reference temperature for 1st order water column toxic decay	(°C)	Lit/Site
RKTOXB	First order sediment bed decay rate for toxic variable	(s^{-1})	Lit/Site
TKTOXB	Reference temperature for 1st order sediment bed toxic decay	(°C)	Lit/Site
VOLTOX	Water surface volitilization rate multiplier		Lit/Site
RMOLTX	Molecular weight for determining volatilization rate		Lit/Site
RKTOXP	Reference photolysis decay rate	(s^{-1})	Lit/Site
SKTOXP	Reference solar radiation for photolysis	($watts/m^2$)	Lit/Site
DIFTOX	Diffusion coefficient for toxicant in sediment bed pore water	(m^2/s)	Lit/Site
NonCohesive/Cohesive Sediment Options			
ISEDINT	0 - Constant initial conditions for Water and Bed 1 - Spatially variable Water column initial conditions 2 - Spatially variable Bed initial conditions 3 - Spatially variable Water column and Bed initial conditions		Lit/Site
ISEDBINT	0 - Spatially varying bed initial conditions in mass/area 1 - Spatially varying bed initial conditions in mass fraction of total sediment mass.		Lit/Site
ISEDWC	0 - Cohesive sed wc/bed exchange based on bottom layer conditions 1 - Cohesive sed wc/bed exchange based on wave/current/sediment boundary layers embedded in bottom layer		Lit/Site
ISMUD	1 - Include cohesive fluid mud viscous effects		Lit/Site
ISNDWC	0 - Noncohesive sediment wc/bed exchange based on bottom layer conditions 1 - Noncohesive sediment wc/bed exchange based on wave/current/sediment boundary layers embedded in bottom layer.		Lit/Site
ISEDVW	0 - Constant or simple concentration dependent cohesive sediment settling velocity >0 Computed: 1 - Huang and Metha, 2 - Shresta and Orlob, 3 - Ziegler and Nesbit		Lit/Site
ISNDVW	0 - Use constant specified nonchoesive sed settling velocities or calculate for class diameter if specified value is negative. >1 - Follow Option 0 procedure but apply hindered settling correction.		Lit/Site
KB	Maximum number of bed layers (excluding active layer)		Lit/Site/Calib
ISEDAL	1 - Activate stationary cohesive mud active layer		Lit/Site
ISNDAL	1 - Activate non-cohesive armoring layer active layer		Lit/Site
Bed Mechanics			
IBMECH	0 - Time invariant constant bed mechanical properites 1 - Simple consolidation calculation with constant coefficients 2 - Simple consolidation with variable coefficients internally computed 3 - Complex consolidation with variable coefficients internally computed		Lit/Site
IMORPH	0 - Constant bed morphology 1 - Active bed morphology: no water entrain/expulsion effects 2 - Active bed morphology: with water entrain/expulsion effects		Lit/Site
HBEDMAX	Top bed layer thickness at which new layer is added or if kbt(i,j) = kb, new layer added and lowest two layers combined	(m)	Lit/Site
BEDPORC	Constant bed porosity for IBMECH=0 or NSED=0		Lit/Site
SEDMDMX	Maximum fluid mud cohesive sediment concentration	(mg/l)	Lit/Site
SEDMDMN	Minimum fluid mud cohesive sediment concentration	(mg/l)	Lit/Site
SEDVDRD	Void ratio of depositing cohesive sediment		Lit/Site
SEDVDRM	Minimum cohesive sediment bed void ratio (IBMECH > 0)		Lit/Site
SEDVDRT	Bed consolodation rate constant (IBMECH = 1,2)	(s^{-1})	Lit/Site
Initial Conditions			
Bed Conditions			
SNDBO	Constant initial noncohesive sediment in bed per unit area (nsnd times)	(g/m^2)	Site
SEDBO	Constant initial cohesive sediment in bed per unit area (nsed times)	(g/m^2)	Site
BEDLINIT	Bed layer thickness	(m)	Site
BEDBINIT	Bed layer bulk density	(g/m^3)	Site
BEDDINIT	Bed layer dry density, porosity or void ratio		Site
ITXINT	Toxic flag for spatially constant/variable water col and bed initial cond		Lit/Site
ITXBDUT	Flag for constant initial bed toxic total or sorbed mass toxic/mass sediment		Site
TOXINTB	Initial bed sediment toxic concentration	(mg/kg)	Site

Housatonic River EFDC Model Parameters

	Definition/Description	Units	Data Source
Volumetric Source/Sinks			
Water Column			
TEMINIT	Temperature	(°C)	Site
SNDO	Constant initial noncohesive sediment conc in water column (nsnd times)	(g/m^3)	Site
SEDO	Constant initial cohesive sediment conc in water column (nsed times)	(g/m^3)	Site
TOXINTW	Initial water column total concentration for nth toxic	ug/l	Site
Physical Domain/Grid	These parameters dictated by scale and channel/floodplain geometry		
CORIOLIS	Constant coriolis parameter in 1/sec		Lit
KC	Number of vertical layers		Site & Calib
IC	Number of cells in i direction		Site & Calib
JC	Number of cells in j direction		Site & Calib
LC	Number of active cells in horizontal + 2		Site & Calib
LVC	Number of variable size horizontal cells		Site & Calib
NDM	Number of domains for horizontal domain decomposition		Site & Calib
LDW	Number of water cells per domain		Site & Calib
XX	Dimesionless layer thicknesss		Site & Calib
DX	Cartesian cell length in x or i direction	(m)	Site & Calib
DY	Cartesion cell length in y or j direction	(m)	Site & Calib
CDLONx	Longitudinal coordinates for cartesian grids		Site
CDLATx	Latitude coordinates for cartesian grids		Site
HDRY	Depth at which cell or flow face becomes dry	(m)	Lit & Site
HWET	Depth at which cell or flow face becomes wet	(m)	Lit & Site
ZBRADJ	Log boundary layer constant or variable roughness height adjustment	(m)	Lit & Site
ZBRCVRT	Log boundary layer variable roughness height conversion		Lit & Site
HMIN	Minimum depth of inputs depths	(m)	Lit & Site
DZC(KC)	Layer thickness ratio		Site & Calib
SubGrid/Channel Modifier			
ISCHAN	1 - Activate subgrid channel model		
IS1DCHAN	1 - Activate 1D channel geometry/grid		
Hydrodyamic Options			
AHO	Horizontal momentum and mass diffusivity	(m^2/s)	Lit/Site
AHD	Dimesionless horizontal momentum diffusivity		Lit/Site
AVO	Molecular kinematic viscosity	(m^2/s)	Lit
ABO	Molecular diffusivity	(m^2/s)	Lit
AVMN	Minimum kinematic eddy viscosity	(m^2/s)	Lit
ABMN	Minimum eddy diffusivity	(m^2/s)	Lit
VKC	Von Karman's Constant		Lit
CTURB1	Turbulence closure constant A1		Lit
CTURB2	Turbulence closure constant B1		Lit
CTE1	Turbulent constant E1		Lit
CTE2	Turbulent constant E2		Lit
CTE3	Turbulent constant E3		Lit
QQMIN	Minimum turbulent intensity squared	(q^2)	Lit
QQLMIN	Minimum turbulent intensity squared time length-scale (l^2)	(M^2)	Lit
DMLMIN	Dimensionless length -scale		Lit
ZBRADJ	Const or variable roughness height adjustment in meters	(m)	Site/Calib
	Vegitative resistance function		Site/Calib
Atmospheric Forcing Functions			
WINDS	Wind Speed	(m/s)	Site
WINDD	Wind Direction (blowing toward)	(degrees)	Site
TDRY	Temperature (Dry Bulb)	(°C)	Site
TWET	Temperature (Wet Bulb)	(°C)	Site
RAIN	Rainfall	(m/s)	Site
EVAP	Evaporation	(m/s)	Site
SOLSWR	Solar Radiation	($J/s/m^2$)	Site

APPENDIX C.3

EFDC TECHNICAL MEMORANDUM: THEORETICAL AND COMPUTATIONAL ASPECTS OF SEDIMENT TRANSPORT IN THE EFDC MODEL

2nd DRAFT

EFDC Technical Memorandum

Theoretical and Computational Aspects of Sediment Transport in the EFDC Model

Prepared for:

US Environmental Protection Agency, Office of Science and Technology
401 M Street SW
Washington, DC 20460

Prepared by:

Tetra Tech, Inc.
10306 Eaton Place
Suite 340
Fairfax, Virginia 22030

August 2000

Table of Contents

1. Introduction

This report summarizes theoretical and computational aspects of the sediment transport formulations used in the EFDC model. Theoretical and computational aspects for the basic EFDC hydrodynamic and generic transport model components are presented in Hamrick (1992). Theoretical and computational aspects of the EFDC water quality-eutrophication model component are presented in Park et al. (1995). The paper by Hamrick and Wu (1997) also summarized computational aspects of the hydrodynamic, generic transport and water quality-eutrophication components of the EFDC model. This report is organized as follows. Chapter 2 summarizes the hydrodynamic and generic transport formulations used in EFDC. Chapter 3 summarizes the solution of the transport equation for suspended cohesive and noncohesive sediment. A discussion of near bed turbulence closure approximations relevant to sediment transport processes is presented in Chapter 4. Chapters 5 and 6 summarize noncohesive and cohesive sediment settling, deposition and resuspension process representations used the sediment transport model component. The representation of the sediment bed and it geomechanical properties are presented in Chapter 7. This report will be subsequently revised to incorporate documentation of the EFDC model's sorptive contaminant transport and fate formulations as well as additional enhancements to the sediment transport formulations which are currently being tested.

2. Summary of Hydrodynamic and Generic Transport Formulations

The EFDC model's hydrodynamic component is based on the three-dimensional hydrostatic equations formulated in curvilinear-orthogonal horizontal coordinates and a sigma or stretched vertical coordinate. The momentum equations are:

$$\begin{aligned}
&\partial_t\left(m_x m_y H u\right)+\partial_x\left(m_y H u u\right)+\partial_y\left(m_x H v u\right)+\partial_z\left(m_x m_y w u\right)-f_e m_x m_y H v \\
&=-m_y H\partial_x\left(p+p_{atm}+f\right)+m_y\left(\partial_x z_b^{*}+z\partial_x H\right)\partial_z p+\partial_z\left(m_x m_y\frac{A_v}{H}\partial_z u\right) \\
&\quad+\partial_x\left(\frac{m_y}{m_x}HA_H\partial_x u\right)+\partial_y\left(\frac{m_x}{m_y}HA_H\partial_y u\right)-m_x m_y c_p D_p\left(u^2+v^2\right)^{1/2}u
\end{aligned} \tag{2.1}$$

$$\begin{aligned}&\P_t\left(m_x m_y H v\right)+\P_x\left(m_y H u v\right)+\P_y\left(m_x H v v\right)+\P_z\left(m_x m_y w v\right)+ f_e m_x m_y H u\\&=-m_x H\P_y\left(p+p_{atm}+f\right)+m_x\left(\P_y z_b^{*}+z\P_y H\right)\P_z p+\P_z\left(m_x m_y\frac{A_v}{H}\P_z v\right)\\&+\P_x\left(\frac{m_y}{m_x}HA_H\P_x v\right)+\P_y\left(\frac{m_x}{m_y}HA_H\P_y v\right)-m_x m_y c_p D_p\left(u^2+v^2\right)^{1/2} v\end{aligned}\tag{2.2}$$

$$m_x m_y f_e = m_x m_y f - u\P_y m_x + v\P_x m_y \tag{2.3}$$

$$\left(\tau_{xz},\tau_{yz}\right)=A_v H^{-1}\P_z(u,v)\tag{2.4}$$

where u and u are the horizontal velocity components in the dimensionless curvilinear-orthogonal horizontal coordinates x and y, respectively. The scale factors of the horizontal coordinates are m_x and m_y. The vertical velocity in the stretched vertical coordinate z is w. The physical vertical coordinates of the free surface and bottom bed are z_s* and z_b* respectively. The total water column depth is H, and f is the free surface potential which is equal to gz_s*. The effective Coriolis acceleration f_e incorporates the curvature acceleration terms, with the Coriolis parameter, f, according to (2.3). The Q terms in (2.1) and (2.2) represent optional horizontal momentum diffusion terms. The vertical turbulent viscosity A_v relates the shear stresses to the vertical shear of the horizontal velocity components by (4.4). The kinematic atmospheric pressure, referenced to water density, is p_{atm}, while the excess hydrostatic pressure in the water column is given by:

$$\P_z p = -gHb = -gH\left(\rho-\rho_o\right)\rho_o^{-1}\tag{2.5}$$

where ρ and ρ_o are the actual and reference water densities and b is the buoyancy. The horizontal turbulent stress on the last lines of (2.1) and (2.2), with A_H being the horizontal turbulent viscosity, are typically retained when the advective acceleration are represented by central differences. The last terms in (2.1) and (2.2) represent vegetation resistance where c_p is a resistance coefficient and D_p is the dimensionless projected vegetation area normal to the flow per unit horizontal area.

The three-dimensional continuity equation in the stretched vertical and curvilinear-orthogonal horizontal coordinate system is:

$$\P_t\left(m_x m_y H\right)+\P_x\left(m_y H u\right)+\P_y\left(m_x H v\right)+\P_z\left(m_x m_y w\right)=Q_H\tag{2.6}$$

with Q_H representing volume sources and sinks including rainfall, evaporation, infiltration and lateral inflows and outflows having negligible momentum fluxes. When the sediment transport

model component operates in a geomorphologic mode, Q_H also includes the volume flux of sediment and water between the sediment bed and the water column. Integration of (2.6) over the water column gives

$$\partial_t (m_x m_y H) + \partial_x (m_y H \bar{u}) + \partial_y (m_x H \bar{v}) = \bar{Q}_H \tag{2.7}$$

the barotropic or external mode continuity equation where the over bars indicate depth averaged quantities. Subtracting (2.7) form (2.6) gives

$$\partial_x (m_y H(u - \bar{u})) + \partial_y (m_x H(v - \bar{v})) + \partial_z (m_x m_y w) = Q_H - \bar{Q}_H \tag{2.8}$$

the internal mode continuity equation.

The generic transport equation for a dissolved or suspended material having a mass per unit volume concentration C, is

$$\begin{aligned} &\partial_t (m_x m_y HC) + \partial_x (m_y HuC) + \partial_y (m_x HvC) + \partial_z (m_x m_y wC) - \partial_z (m_x m_y w_{sc} C) \\ &= \partial_x \left(\frac{m_y}{m_x} HK_H \partial_x C \right) + \partial_y \left(\frac{m_x}{m_y} HK_H \partial_y v \right) + \partial_z \left(m_x m_y \frac{K_v}{H} \partial_z C \right) + Q_c \end{aligned} \tag{2.9}$$

where K_v and K_H are the vertical and horizontal turbulent diffusion coefficients, respectively, w_{sc} is a positive settling velocity went C represents a suspended material, and Q_c represents external sources and sinks and reactive internal sources and sinks.

The solution of the momentum equations, (2.1) and (2.2) and the transport equation (2.9), requires the specification of the vertical turbulent viscosity, A_v, and diffusivity, K_v. To provide the vertical turbulent viscosity and diffusivity, the second moment turbulence closure model developed by Mellor and Yamada (1982) and modified by Galperin *et al* (1988) and Blumberg *et al* (1988) is used. The MY model relates the vertical turbulent viscosity and diffusivity to the turbulent intensity, q, a turbulent length scale, l, and a turbulent intensity and length scaled based Richardson number, R_q, by:

$$A_v = f_A q l$$

$$f_A = \frac{A_o\left(1 + R_1^{-1} R_q\right)}{\left(1 + R_2^{-1} R_q\right)\left(1 + R_3^{-1} R_q\right)}$$

$$A_o = A_1\left(1 - 3C_1 - \frac{6A_1}{B_1}\right) = \frac{1}{B_1^{1/3}}$$

$$R_1^{-1} = 3A_2 \frac{\left(B_2 - 3A_2\right)\left(1 - \frac{6A_1}{B_1}\right) - 3C_1\left(B_2 + 6A_1\right)}{\left(1 - 3C_1 - \frac{6A_1}{B_1}\right)}$$

$$R_2^{-1} = 9A_1A_2 \qquad (2.10)$$

$$R_3^{-1} = 3A_2\left(6A_1 + B_2\right)$$

$$K_v = f_K q l$$

$$f_K = \frac{K_o}{\left(1 + R_3^{-1} R_q\right)} \qquad (2.11)$$

$$K_o = A_2\left(1 - \frac{6A_1}{B_1}\right)$$

$$R_q = -\frac{gH\partial_z b}{q^2}\frac{l^2}{H^2} \qquad (2.12)$$

where the so-called stability functions, f_A and f_K, account for reduced and enhanced vertical mixing or transport in stable and unstable vertically density stratified environments, respectively. Mellor and Yamada (1982) specify the constants A_1, B_1, C_1, A_2, and B_2 as 0.92, 16.6, 0.08, 0.74, and 10.1, respectively.

The turbulent intensity and the turbulent length scale are determined by a pair of transport equations:

$$\begin{aligned}
&\partial_t\left(m_x m_y H q^2\right) + \partial_x\left(m_y H u q^2\right) + \partial_y\left(m_x H v q^2\right) + \partial_z\left(m_x m_y w q^2\right) \\
&\quad = \partial_z\left(m_x m_y \frac{A_q}{H}\partial_z q^2\right) - 2m_x m_y \frac{H q^3}{B_1 l} \\
&+ 2m_x m_y\left(\frac{A_v}{H}\left(\left(\partial_z u\right)^2 + \left(\partial_z v\right)^2\right) + h_p c_p D_p\left(u^2 + v^2\right)^{3/2} + g K_v \partial_z b\right) + Q_q
\end{aligned} \qquad (2.13)$$

$$\begin{aligned}
&\partial_t\left(m_x m_y H q^2 l\right)+\partial_x\left(m_y H u q^2 l\right)+\partial_y\left(m_x H v q^2 l\right)+\partial_z\left(m_x m_y w q^2 l\right)\\
&=\partial_z\left(m_x m_y \frac{A_q}{H}\partial_z\left(q^2 l\right)\right)-m_x m_y \frac{H q^3}{B_1}\left(1+E_2\left(\frac{l}{\kappa H z}\right)^2+E_3\left(\frac{l}{\kappa H(1-z)}\right)^2\right)\\
&+m_x m_y E_1 l\left(\frac{A_v}{H}\left(\left(\partial_z u\right)^2+\left(\partial_z v\right)^2\right)+g K_v \partial_z b+\eta_p c_p D_p\left(u^2+v^2\right)^{3/2}\right)+Q_l
\end{aligned} \tag{2.14}$$

where (E_1, E_2, E_3) = (1.8, 1.33, 0.25). The third on the last line of each equation represents net turbulent energy production by vegetation drag where η_p is a production efficiency factor have a value less than one. The terms Q_q and Q_l may represent additional source-sink terms such as subgrid scale horizontal turbulent diffusion. The vertical diffusivity, A_q, is set to $0.2ql$ as recommended by Mellor and Yamada (1982) For stable stratification, Galperin *et al* (1988) suggest limiting the length scale such that the square root of R_q is less than 0.52. When horizontal turbulent viscosity and diffusivity are included in the momentum and transport equations, they are determined independently using Smagorinsky's (1963) subgrid scale closure formulation.

Vertical boundary conditions for the solution of the momentum equations are based on the specification of the kinematic shear stresses, equation (2.4), at the bed and the free surface. At the free surface, the *x* and *y* components of the stress are specified by the water surface wind stress

$$\left(\tau_{xz},\tau_{yz}\right)=\left(\tau_{sx},\tau_{sy}\right)=c_s\sqrt{U_w^2+V_w^2}\left(U_w,V_w\right) \tag{2.15}$$

where U_w and V_w are the x and y components of the wind velocity at 10 meters above the water surface. The wind stress coefficient is given by:

$$c_s=0.001\frac{\rho_a}{\rho_w}\left(0.8+0.065\sqrt{U_w^2+V_w^2}\right) \tag{2.16}$$

for the wind velocity components in meters per second, with ρ_a and ρ_w denoting air and water densities respectively. At the bed, the stress components are presumed to be related to the near bed or bottom layer velocity components by the quadratic resistance formulation

$$\left(\tau_{xz},\tau_{yz}\right)=\left(\tau_{bx},\tau_{by}\right)=c_b\sqrt{u_1^2+v_1^2}\left(u_1,v_1\right) \tag{2.17}$$

where the 1 subscript denotes bottom layer values. Under the assumption that the near bottom velocity profile is logarithmic at any instant of time, the bottom stress coefficient is given by

$$c_b=\left(\frac{\kappa}{\ln\left(\Delta_1/2z_o\right)}\right)^2 \tag{2.18}$$

where k, is the von Karman constant, D_1 is the dimensionless thickness of the bottom layer, and $z_o=z_o^*/H$ is the dimensionless roughness height. Vertical boundary conditions for the turbulent kinetic energy and length scale equations are:

$$q^2 = B_1^{2/3}|\tau_s| \quad : \quad z = 1 \tag{2.19}$$

$$q^2 = B_1^{2/3}|\tau_b| \quad : \quad z = 0 \tag{2.20}$$

$$l = 0 \quad : \quad z = 0,1 \tag{2.21}$$

where the absolute values indicate the magnitude of the enclosed vector quantity. Equations (2.17) and (2.18) can become inappropriate under a number of conditions associated with either or both high near bottom sediment concentrations and high frequency surface wave activity. The quantification of sediment and wave effects on the bottom stress is discussed in Chapter 4.

3. Solution of the Sediment Transport Equation

The EFDC model uses a high order upwind difference solution scheme for the advective terms in the transport equation. Although the scheme is designed to minimize numerical diffusion, a small amount of horizontal diffusion remains inherent in the scheme. Due the small inherent numerical diffusion, the physical horizontal diffusion terms in (2.9) are omitted as to give:

$$\begin{aligned} &\partial_t(m_x m_y H S_j) + \partial_x(m_y H u S_j) + \partial_y(m_x H v S_j) + \partial_z(m_x m_y w S_j) \\ &-\partial_z(m_x m_y w_{sj} S_j) = \partial_z\left(m_x m_y \frac{K_V}{H}\partial_z S_j\right) + Q_{sj}^E + Q_{sj}^I \end{aligned} \tag{3.1}$$

where S_j represents the concentration of the jth sediment class and the source-sink term has been split into an external part, which would include point and nonpoint source loads, and internal part which could include reactive decay of organic sediments or the exchange of mass between sediment classes if floc formation and destruction were simulated. Vertical boundary conditions for (3.1) are:

$$\begin{aligned} -\frac{K_V}{H}\partial_z S_j - w_s S &= J_{jo} : z \approx 0 \\ -\frac{K_V}{H}\partial_z S_j - w_{sj} S_j &= 0 : z = 1 \end{aligned} \tag{3.2}$$

where J_o is the net water column-bed exchange flux defined as positive into the water column.

The numerical solution of (3.1) utilizes a fractional step procedure. The first step advances the concentration due to advection and external sources and sinks having corresponding volume fluxes by

$$H^{n+1}S^{*} = H^{n}S^{n} + \frac{\theta}{m_x m_y}\left(Q_{sj}^{E}\right)^{n+1/2}$$
$$-\frac{\theta}{m_x m_y}\left(\partial_x\left(m_y (Hu)^{n+1/2} S^{n}\right) + \partial_y\left(m_x (Hv)^{n+1/2} S^{n}\right) + \partial_z\left(m_x m_y w^{n+1/2} S^{n}\right)\right) \tag{3.3}$$

where *n* and *n+1* denote the old and new time levels and * denotes the intermediate fractional step results. The portion of the source and sink term, associated with volumetric sources and sinks is included in the advective step for consistency with the continuity constraint. This term, as well as the advective field (*u*,*v*,*w*), is defined as intermediate in time between the old and new time levels consistent with continuity. Note that the sediment class subscripts have be dropped for clarity. The advection set uses the antidiffusive MPDATA scheme (Smolarkiewicz and Clark, 1986) with optional flux corrected transport (Smolarkiewicz and Grabowski, 1990).

The second fractional settling step is given by

$$S^{**} = S^{*} + \frac{\theta}{H^{n+1}}\partial_z\left(w_s S^{**}\right) \tag{3.4}$$

which is solved by a fully implicit upwind difference scheme with an optional antidiffusion correction across internal water column layer interfaces. For the bottom bed adjacent layer, (3.4) is written as:

$$S_1^{**} = S_1^{*} + \frac{\theta}{\Delta_1 H^{n+1}}\left(w_s S^{**}\right)_2 - \frac{\theta}{\Delta_z H^{n+1}}\left(w_s S^{**}\right)_1 \tag{3.5}$$

The water column-bed flux (3.2) can be written as

$$-\frac{K_V}{H}\partial_z S_j - w_s S = J_o = w_r S_r - P_d w_s S \tag{3.6}$$

where the product, $w_r S_r$ symbolically represents the resuspension flux and P_d the probability of deposition which is less than or equal to one. Since the remaining step will represent diffusion, for solution efficiency, the diffusive flux at the bed in (3.6) is set to zero in the settling and subsequent diffusion set. Equation (3.5) then becomes

$$\left(1 + \frac{\theta P_d w_s}{\Delta_z H^{n+1}}\right) S_1^{**} = S_1^{*} + \frac{\theta}{\Delta_1 H^{n+1}}\left(w_s S^{**}\right)_2 + \frac{\theta}{\Delta_z H^{n+1}} w_r S_r \tag{3.7}$$

In the actual EFDC code, if the net bed flux, J_o is positive, it is limited such that only the current top layer of the bed can be completely resuspended in single time step. The remaining fractional step is an implicit diffusion step

$$S^{n+1} = S^{**} + \theta\partial_z\left(\left(\frac{K_V}{H^2}\right)^{n+1}\partial_z S^{n+1}\right) \tag{3.8}$$

with zero diffusive fluxes at the bed and water surface.

4. Near Bed Turbulence Closure

The proper formulation of hydrodynamic and sediment boundary layer parameterization appropriate for representing the bottom stress and the water column-bed exchange of sediment under conditions including high frequency surface waves and high near bed suspended sediment gradients should be based upon the near bed turbulent kinetic energy balance. The near bed balance assumes an equilibrium between production of turbulence by shear stresses, vegetation drag, and unstable density stratification, the suppression of turbulence by stable stratification, and the dissipation. The turbulent kinetic energy equation (2.13) reduces to

$$\frac{A_v}{H}\left(\left(\partial_z u\right)^2+\left(\partial_z v\right)^2\right)+\beta_p c_p D_p\left(u^2+v^2\right)^{3/2}+gK_v\partial_z b=\frac{Hq^3}{B_1 l} \tag{4.1}$$

Multiplying (4.1) by A_v/H and using (2.4) gives

$$\left(\tau_{xz}^2+\tau_{yz}^2\right)+\beta_p c_p D_p\frac{A_v}{H}\left(u^2+v^2\right)^{3/2}+gK_v\frac{A_v}{H}\partial_z b=\frac{A_v}{H}\frac{Hq^3}{B_1 l} \tag{4.2}$$

In the absence of vegetation and stratification, evaluation of (4.2) at the bed, using (2.10) gives

$$\left(\tau_{xz}^2+\tau_{yz}^2\right)_b=\left|\tau_b\right|^2=\frac{1}{B_1^{1/3}}q\frac{l}{H}\frac{Hq^3}{B_1 l}=\frac{q^4}{B_1^{4/3}} \tag{4.3}$$

recovering the boundary condition (2.20).

For the general case, the definition of A_v is introduced into (4.2) to give

$$q^4-B_1\left(gH\frac{l}{H}\frac{K_v}{H}\partial_z b+\beta_p c_p D_p\frac{l}{H}\left(u^2+v^2\right)^{3/2}\right)q-\frac{B_1}{f_A}\left(\tau_{xz}^2+\tau_{yz}^2\right)=0 \tag{4.4}$$

Near the bed for three-dimensional model applications and over the depth for two-dimensional applications, the turbulent length scale can be specified by the algebraic relationship

$$\frac{l}{H}=\kappa z\left(1-z\right)^l \tag{4.5}$$

If high frequency surface waves are present, the shear stress can be decomposed into current and wave components

$$\begin{aligned}\tau_{xz}&=\tau_c\cos\gamma_c+\tau_w\cos\gamma_w\\ \tau_{yz}&=\tau_c\sin\gamma_c+\tau_w\sin\gamma_w\end{aligned} \tag{4.6}$$

where τ_c and τ_w are the current and wave shear stress magnitudes. Evaluating the stress term in (4.4) gives

$$\left(t_{xz}^2 + t_{yz}^2\right) = t_c^2 + t_w^2 + 2\left(\cos\gamma_c \cos\gamma_w + \sin\gamma_c \sin\gamma_w\right) t_c t_w \tag{4.7}$$

Assuming the wave shear stress to be periodic

$$\begin{aligned} t_w &= t_{wm} \sin(\omega t) \\ \gamma_w &= \gamma_{wm} \mathrm{sgn}\left(\sin(\omega t)\right) \end{aligned} \tag{4.8}$$

the mean square stress average over the wave period is given by

$$\left\langle t_{xz}^2 + t_{yz}^2 \right\rangle = t_c^2 + \frac{1}{2} t_{wm}^2 + \frac{4}{\pi} t_c t_{wm} \cos\left(\gamma_c - \gamma_{wm}\right) \tag{4.9}$$

For wave periods much smaller than the time step of the numerical integration, (4.4) is well approximated using (4.9) as

$$\begin{aligned} & q^4 - B_1 \left(gH \frac{l}{H} \frac{K_v}{H} \nabla_z b + \alpha_p c_p D_p \frac{l}{H} \left(u^2 + v^2\right)^{3/2} \right) q \\ & - \frac{B_1}{f_A} \left(t_c^2 + \frac{1}{2} t_{wm}^2 + \frac{4}{\pi} t_c t_{wm} \cos\left(\gamma_c - \gamma_{wm}\right) \right) = 0 \end{aligned} \tag{4.10}$$

The buoyancy gradient near the bed is primarily due to gradients in suspended sediment concentration with the effect of sediment on density given by

$$\rho = \left(\frac{\varepsilon}{1+\varepsilon}\right) \rho_w + \left(\frac{1}{1+\varepsilon}\right) \rho_s = \left(\frac{\varepsilon}{1+\varepsilon}\right) \rho_w + S \tag{4.11}$$

where ε is the void ratio of the sediment water mixture and S is the mass concentration of sediment. The buoyancy can be expressed in terms of the sediment concentration using

$$b = \frac{\rho - \rho_w}{\rho_w} = \left(\frac{\rho_s - \rho_w}{\rho_w \rho_s} \right) S = \alpha S \tag{4.12}$$

with (4.10) becoming

$$\begin{aligned} & q^4 - B_1 \left(\alpha g H \frac{l}{H} \frac{K_v}{H} \nabla_z S + \alpha_p c_p D_p \frac{l}{H} \left(u^2 + v^2\right)^{3/2} \right) q \\ & - \frac{B_1}{f_A} \left(t_c^2 + \frac{1}{2} t_{wm}^2 + \frac{4}{\pi} t_c t_{wm} \cos\left(\gamma_c - \gamma_{wm}\right) \right) = 0 \end{aligned} \tag{4.13}$$

Equation (4.13) provides an algebraic equation for specifying the turbulent intensity q at any level in the hydrodynamic and sediment boundary layers. Since the boundary layer parameter are recalculated at each time step of the hydrodynamic model integration, the solution of (4.13) can be approximated by

$$\left(q^4\right)^{n+1} = B_1\left(\alpha g H \frac{l}{H}\frac{K_v}{H}\nabla_z S q + \beta_p c_p D_p \frac{l}{H}\left(u^2+v^2\right)^{3/2} q\right)^n + \frac{B_1}{f_A}\left(\tau_c^2 + \frac{1}{2}\tau_{wm}^2 + \frac{4}{\pi}\tau_c\tau_{wm}\cos(\phi_c - \phi_{wm})\right)^n \tag{4.14}$$

where *n+1* and *n* denote the new and old time levels, respectively. Since the vertical gradient of the sediment concentration is generally negative, there is low possibility of the right side of (4.13) also being negative. In such and event, the turbulent intensity is set to a small value on the order of 1E-4 meters/second.

5. Noncohesive Sediment Settling, Deposition and Resuspension

Noncohesive inorganic sediments settle as discrete particles, with hindered settling and multiphase interactions becoming important in regions of high sediment concentration near the bed. At low concentrations, the settling velocity for the jth noncohesive sediment class corresponds to the settling velocity of a discrete particle:

$$w_{sj} = w_{soj} \tag{5.1}$$

Useful expressions for the discrete particle settling velocity which depends on the sediment density, effective grian diameter, and fluid kinematic viscosity, provide by van Rijn (1984b) are:

$$\frac{w_{soj}}{\sqrt{g' d_j}} = \begin{cases} \dfrac{R_{dj}}{18} & : \quad d \le 100\,mm \\ \dfrac{10}{R_{dj}}\left(\sqrt{1+0.01R_{dj}^2}-1\right) & : \quad 100\,mm < d_j \le 1000\,mm \\ 1.1 & : \quad d_j > 1000\,mm \end{cases} \tag{5.2}$$

where

$$g' = g\left(\frac{\rho_{sj}}{\rho_w} - 1\right) \tag{5.3}$$

is the reduced gravitational acceleration and

$$R_{dj} = \frac{d_j\sqrt{g' d_j}}{\nu} \tag{5.4}$$

is a the sediment grain densimetric Reynolds number.

At higher concentrations and hindering settling conditions, the settling velocity is less than the discrete velocity and can be expressed in the form

$$w_{sj} = \left(1 - \sum_i^I \frac{S_i}{\rho_{si}}\right)^n w_{soj} \tag{5.5}$$

where ρ_s is the sediment particle density with values of n ranging from 2 (Cao et al., 1996) to 4 (Van Rijn, 1984). The expression (5.2) is approximated to within 5 per cent by

$$w_{sj} = \left(1 - n\sum_i^I \frac{S_i}{\rho_{si}}\right) w_{soj} \tag{5.6}$$

for total sediment concentrations up to 200,000 mg/liter. For total sediment concentrations less than 25,000 mg/liter, neglect of the hindered settling correction results in less than a 5 per cent error in the settling velocity, which is well within the range of uncertainty in parameters used to estimate the discrete particle settling velocity.

Noncohesive sediment is transported as bed load and suspended load. The initiation of both modes of transport begins with erosion or resuspension of sediment from the bed when the bed stress, τ_b, exceeds a critical stress referred to as the Shield's stress, τ_{cs}. The Shield's stress depends upon the density and diameter of the sediment particles and the kinematic viscosity of the fluid and can be expressed in empirical dimensionless relationships of the form:

$$\theta_{csj} = \frac{\tau_{csj}}{g' d_j} = \frac{u_{*csj}^2}{g' d_j} = f\left(R_{dj}\right) \tag{5.7}$$

Useful numerical expressions of the relationship (5.5), provided by van Rijn (1984b), are:

$$\theta_{csj} = \begin{cases} 0.24\left(R_{dj}^{2/3}\right)^{-1} & : \quad R_{dj}^{2/3} < 4 \\ 0.14\left(R_{dj}^{2/3}\right)^{-0.64} & : \quad 4 \le R_{dj}^{2/3} < 10 \\ 0.04\left(R_{dj}^{2/3}\right)^{-0.1} & : \quad 10 \le R_{dj}^{2/3} < 20 \\ 0.013\left(R_{dj}^{2/3}\right)^{0.29} & : \quad 20 \le R_{dj}^{2/3} < 150 \\ 0.055 & : \quad R_{dj}^{2/3} \ge 150 \end{cases} \tag{5.8}$$

A number of approaches have been used to distinguish wheather a particular sediment size class is transported as bed load or suspended load under specific local flow conditions characherized by the bed stress or bed shear velocity:

$$u_* = \sqrt{\tau_b} \tag{5.9}$$

The approach proposed by van Rijn (1984a) is adopted in the EFDC model and is as follows. When the bed velocity is less than the critical shear velocity

$$u_{*csj} = \sqrt{\tau_{csj}} = \sqrt{g' d_j \theta_{csj}} \tag{5.10}$$

no erosion or resuspension takes place and there is no bed load transport. Sediment in suspension under this condition will deposit to the bed as will be subsequently discussed. When the bed shear velocity exceeds the critial shear velocity but remains less than the settling velocity,

$$u_{*csj} < u_* < w_{soj} \tag{5.11}$$

sediment will be eroded from the bed and transported as bed load. Sediment in suspension under this condition will deposit to the bed. When the bed shear velocity exceeds both the critical shear velocity and the settling velocity, bed load transport ceases and the eroded or resuspended sediment will be transported as suspended load. These various transport modes are further illustrated by reference to Figure 1, which shows dimensional forms of the settling velocity relationship (5.2) and the critical Shield's shear velocity (5.10), determined using (5.8) for sediment with a specific gravity of 2.65. For grain diameters less than approximately 1.3E-4 m (130 um) the settling velocity is less than the critical shear velocity and sediment resuspend from the bed when the bed shear velocity exceeds the critical shear velocity will be transported entirely as suspended load. For grain diameters greater than 1.3E-4 m, eroded sediment be transported by bed load in the region corresponding to (5.11) and then as suspended load when the bed shear velocity exceeds the settling velocity.

In the EFDC model, the preceding set of rules are used to deterimne the mode of transport of multiple size classes of noncohesive sediment. Bed load transport is determined using a general bed load transport rate formula:

$$\frac{q_B}{\rho_s d\sqrt{g'd}} = \Phi(\theta, \theta_{cs}) \tag{5.12}$$

where q_B is the bed load transport rate (mass per unit time per unit width) in the direction of the near bottom horizontal flow velocity vector. The function Φ depends on the Shield's parameter

$$\theta = \frac{\tau_b}{g' d_j} = \frac{u_*^2}{g' d_j} \tag{5.13}$$

and the critical Shield's parameter defined by (5.7) and (5.8). A number of bed load transport formulas explicity incorprate the settling velocity. However, since both the critical Shield's parameter and the settling velocity are unique functions of the sediment grain densimetric Reynolds number, the settling velocity can also be expressed as a funtion of the critical Shield's parameter with (5.12) remaining an appropriate representation.

A number of bed load formulations developed for riverine prediction (Ackers and White, 1973; Laursen, 1958; Yang, 1973; Yang and Molinas, 1982) do not readily conform to (1) and were not incorporated as options in the EFDC model. Two widely used bed load formulations wihch do conform to (5.12) are the Meyer-Peter and Muller (1948) and Bagnold (1956) formulas and their derivatives (Raudkivi, 1967; Neilson, 1992; Reid and Frostick, 1994) which have the general form

$$\Phi(q,q_{cs}) = f(q - q_{cs})^a \left(\sqrt{q} - g\sqrt{q_{cs}}\right)^b \tag{5.14}$$

where

$$f = f(q_{cs}) \quad or \quad f(R_d) \tag{5.15}$$

The Meyer-Peter and Muller formulations are typified by

$$\Phi = f(q - q_{cs})^{3/2} \tag{5.16}$$

while Bagnold formulations are typified by

$$\Phi = f(q - q_{cs})\left(\sqrt{q} - g\sqrt{q_{cs}}\right) \tag{5.17}$$

with Bagnold's original formula having g equal to zero. The Meyer-Peter and Muller formulation has been extended to heterogeneous beds by Suzuki et al. (1998), while Bagnold's formula has been similarly extended by van Niekerk et al. (1992). The bed load formulation by van Rijn (1984a) having the form

$$\begin{aligned} \Phi &= f(q - q_{cs})^{2.1} \\ f &= \frac{0.053}{R_d^{1/5} q_{cs}^{2.1}} \end{aligned} \tag{5.18}$$

has been incorporated int the CH3D-SED model and modified for heterogeneous beds by Spasojevic and Holly (1994). Equation (5.18) can be implemented in the EFDC model with an appropriately specified f. A modified formulation of the Einstein bed load function (Einstein, 1950) which confoms to (5.12) and (5.14) has been presented by Rahmeyer (1999) and will be later incorporated into the EFDC model.

The procedure for coupling bed load transport with the sediment bed in the EFDC model is as follows. First, the magnitude of the bed load mass flux per unit width is calculated according to (5.12) at horizontal model cell centers, denoted by the subscript *c*. The cell center flux is then transformed into cell center vector components using

$$\begin{aligned} q_{bcx} &= \frac{u}{\sqrt{u^2 + v^2}} q_{bc} \\ q_{bcy} &= \frac{v}{\sqrt{u^2 + v^2}} q_{bc} \end{aligned} \tag{5.19}$$

where u and v are the cell center horizontal velocities near the bed. Cell face mass fluxes are determined by down wind projection of the cell center fluxes

$$q_{bfx} = (q_{bcx})_{upwind}$$
$$q_{bfy} = (q_{bcy})_{upwind} \qquad (5.20)$$

where the subscript *upwind* denotes the cell center upwind of the *x* normal and *y* normal cell faces. The net removal or accumulation rate of sediment material from the deposited bed underlying a water cell is then given by:

$$m_x m_y J_b = (m_y F_{bfx})_e - (m_y F_{bfx})_w + (m_x F_{bfy})_n - (m_x F_{bfy})_s \qquad (5.21)$$

where J_b is the net removal rate (gm/m*m-sec) from the bed, m_x and m_y are *x* and *y* dimensions of the cell, and the compass direction subscripts define the four cell faces. The implementation of (5.19) through (5.21) in the EFDC code includes logic to limit the out fluxes (5.20) over a time step, such that the time integrated mass flux from the bed does not exceed bed sediment available for erosion or resuspension.

Under conditions when the bed shear velocity exceeds the settling velocity and critical Shield's shear velocity, noncohesive sediment will be resuspended and transported as suspended load. When the bed shear velocity falls below both settling velocity and the critical Shield's shear velocity, suspended sediment will deposit to the bed. A consistent formulation of these processes can be developed using the concept of a near bed equilibrium sediment concentration. Under steady, uniform flow and sediment loading conditions, an equilibrium distribution of sediment in the water column tends to be established, with the resuspension and deposition fluxes canceling each other. Using a number of simplifying assumptions, the equilibrium sediment concentration distribution in the water column can be expressed analytically in terms of the near bed reference or equilibrium concentration, the settling velocity and the vertical turbulent diffusivity. For unsteady or spatially varying flow conditions, the water column sediment concentration distribution varies in space and time in response to sediment load variations, changes in hydrodynamic transport, and associated nonzero fluxes across the water column-sediment bed interface. An increase or decrease in the bed stress and the intensity of vertical turbulent mixing will result in net erosion or deposition, respectively, at a particular location or time.

To illustrate how an appropriate suspended noncohesive sediment bed flux boundary condition can be established, consider the approximation to the sediment transport equation (3.1) for nearly uniform horizontal conditions

$$\partial_t (HS) = \partial_z \left(\frac{K_v}{H} \partial_z S + w_s S \right) \qquad (5.22)$$

Integrating (5.22) over the depth of the bottom hydrodynamic model layer gives

$$\partial_t (\Delta H \bar{S}) = J_0 - J_\Delta \qquad (5.23)$$

where the over bar denotes the mean over the dimensionless layer thickness, *D*. Subtracting (5.23) from (5.22) gives

$$\partial_t (HS') = \partial_z \left(\frac{K_v}{H} \partial_z S + w_s S \right) - \left(\frac{J_0 - J_\Delta}{\Delta} \right) \tag{5.24}$$

Assuming that the rate of change of the deviation of the sediment concentration from the mean is small

$$\partial_t (HS') << \partial_t \left(H\bar{S} \right) \tag{5.25}$$

allows (5.24) to be approximated by

$$\partial_z \left(\frac{K_v}{H} \partial_z S + w_s S \right) = \left(\frac{J_0 - J_\Delta}{\Delta} \right) \tag{5.26}$$

Integrating (5.26) once gives

$$\frac{K_v}{H} \partial_z S + w_s S = \left(J_0 - J_\Delta \right) \frac{z}{\Delta} - J_0 \tag{5.27}$$

Very near the bed, (5.27) can be approximated by

$$\frac{K_v}{H} \partial_z S + w_s S = -J_0 \tag{5.28}$$

Neglecting stratification effects and using the results of Chapter 4, the near bed diffusivity is approximately

$$\frac{K_v}{H} = K_o q \frac{l}{H} \cong u_* \kappa z \tag{5.29}$$

Introducing (5.29) into (5.28) gives

$$\partial_z S + \frac{R}{z} S = -\frac{R}{z} \frac{J_o}{w_s} \tag{5.30}$$

where

$$R = \frac{w_s}{u_* \kappa} \tag{5.31}$$

is the Rouse parameter. The solution of (5.30) is

$$S = -\frac{J_o}{w_s} + \frac{C}{z^R} \tag{5.32}$$

The constant of integration is evaluated using

$$S = S_{eq} \quad : \quad z = z_{eq} \quad and \quad J_o = 0 \tag{5.33}$$

which sets the near bed sediment concentration to an equilibrium value, defined just above the bed under no net flux condition. Using (5.33), equation (5.32) becomes

$$S = \left(\frac{z_{eq}}{z} \right)^R S_{eq} - \frac{J_o}{w_s} \tag{5.34}$$

For nonequilibrium conditions, the net flux is given by evaluating (5.34) at the equilibrium level

$$J_o = w_s \left(S_{eq} - S_{ne} \right) \tag{5.35}$$

where S_{ne} is the actual concentration at the reference equilibrium level. Equation (5.35) clearly indicates that when the near bed sediment concentration is less than the equilibrium value a net flux from the bed into the water column occurs. Likewise when the concentration exceeds equilibrium, a net flux to the bed occurs.

For the relationship (5.35) to be useful in a numerical model, the bed flux must be expressed in terms of the model layer mean concentration. For a three-dimensional application, (5.34) can be integrated over the bottom model layer to give

$$J_o = w_s \left(\bar{S}_{eq} - \bar{S} \right) \tag{5.36}$$

where

$$\begin{aligned} \bar{S}_{eq} &= \frac{\ln\left(\Delta z_{eq}^{-1}\right)}{\left(\Delta z_{eq}^{-1} - 1\right)} S_{eq} : R = 1 \\ \bar{S}_{eq} &= \frac{\left(\left(\Delta z_{eq}^{-1}\right)^{1-R} - 1\right)}{(1-R)\left(\Delta z_{eq}^{-1} - 1\right)} S_{eq} : R \neq 1 \end{aligned} \tag{5.37}$$

defines an equivalent layer mean equilibrium concentration in terms of the near bed equilibrium concentration. The corresponding quantities in the numerical solution bottom boundary condition (3.6) are

$$\begin{aligned} w_r S_r &= w_s \bar{S}_{eq} \\ P_d w_s &= w_s \end{aligned} \tag{5.38}$$

If the dimensionless equilibrium elevation, z_{eq} exceeds the dimensionless layer thickness, (5.19) can be modified to

$$\bar{S}_{eq} = \frac{\ln\left(M\Delta z_{eq}^{-1}\right)}{\left(M\Delta z_{eq}^{-1} - 1\right)} S_{eq} : R = 1$$

$$\bar{S}_{eq} = \frac{\left(\left(M\Delta z_{eq}^{-1}\right)^{1-R} - 1\right)}{(1-R)\left(M\Delta z_{eq}^{-1} - 1\right)} S_{eq} : R \neq 1 \qquad (5.39)$$

where the over bars in (5.36) and (5.38) implying an average of the first *M* layers above the bed.

For two-dimensional, depth averaged model application, a number of additional considerations are necessary. For depth average modeling, the equivalent of (5.27) is

$$\frac{K_v}{H} \partial_z S + w_s S = -J_o (1 - z) \qquad (5.40)$$

Neglecting stratification effects and using the results of Chapter 4, the diffusivity is

$$\frac{K_v}{H} = K_o q \frac{l}{H} \cong u_* \kappa z (1 - z)^l \qquad (5.41)$$

Introducing (5.41) into (5.40) gives

$$\partial_z S + \frac{R}{z(1-z)^l} S = -\frac{R(1-z)^{1-l}}{z} \frac{J_o}{w_s} \qquad (5.42)$$

A close form solution of (5.42) is possible for λ equal to zero. Although the resulting diffusivity is not as reasonable as the choice of λ equal to one, the resulting vertical distribution of sediment is much more sensitive to the near bed diffusivity distribution than the distribution in the upper portions of the water column. For λ equal to zero, the solution of (5.42) is

$$S = -\left(1 - \frac{Rz}{(1+R)}\right) \frac{J_o}{w_s} + \frac{C}{z^R} \qquad (5.43)$$

Evaluating the constant of integration using (5.43) gives

$$S = \left(\frac{z_{eq}}{z}\right)^R S_{eq} - \left(1 - \frac{Rz}{(1+R)}\right) \frac{J_o}{w_s} \qquad (5.44)$$

For nonequilibrium conditions, the net flux is given by evaluating (5.44) at the equilibrium level

$$J_o = w_s \left(\frac{(1+R)}{1 + R(1 - z_{eq})}\right) \left(S_{eq} - S_{ne}\right) \qquad (5.45)$$

where S_{ne} is the actual concentration at the reference equilibrium level. Since z_{eq} is on the order of the sediment grain diameter divided by the depth of the water column, (5.45) is essentially

equivalent (5.35). To obtain an expression for the bed flux in terms of the depth average sediment concentration, (5.44) is integrated over the depth to give

$$J_o = w_s\left(\frac{2(1+R)}{2+R(1-z_{eq})}\right)(\bar{S}_{eq} - \bar{S}) \tag{5.46}$$

where

$$\bar{S}_{eq} = \frac{\ln(z_{eq}^{-1})}{(z_{eq}^{-1}-1)} S_{eq} : R = 1$$

$$\bar{S}_{eq} = \frac{(z_{eq}^{R-1}-1)}{(1-R)(z_{eq}^{-1}-1)} S_{eq} : R \neq 1 \tag{5.47}$$

The corresponding quantities in the numerical solution bottom boundary condition (3.6) are

$$w_r S_r = w_s\left(\frac{2(1+R)}{2+R(1-z_{eq})}\right)\bar{S}_{eq}$$

$$P_d w_s = \left(\frac{2(1+R)}{2+R(1-z_{eq})}\right) w_s \tag{5.48}$$

When multiple sediment size classes are simulated, the equilibrium concentrations given by (5.37), (5.39), and (5.47) are adjusted by multiplying by their respective sediment volume fractions in the surface layer of the bed.

The specification of the water column-bed flux of noncohesive sediment has been reduced to specification of the near bed equilibrium concentration and its corresponding reference distance above the bed. Garcia and Parker (1991) evaluated seven relationships, derived by combinations of analysis and experiment correlation, for determining the near bed equilibrium concentration as well as proposing a new relationship. All of the relationships essential specify the equilibrium concentration in terms of hydrodynamic and sediment physical parameters

$$S_{eq} = S_{eq}(d, \rho_s, \rho_w, w_s, u_*, \nu) \tag{5.49}$$

including the sediment particle diameter, the sediment and water densities, the sediment settling velocity, the bed shear velocity, and the kinematic molecular viscosity of water. Garcia and Parker concluded that the representations of Smith and McLean (1977) and Van Rijn (1984b) as well as their own proposed representation perform acceptably when tested against experimental and field observations.

Smith and McLean's formula for the equilibrium concentration is

$$S_{eq} = \rho_s \frac{0.65 g_o T}{1 + g_o T} \tag{5.50}$$

where g_o is a constant equal to 2.4E-3 and T is given by

$$T = \frac{\tau_b - \tau_{cs}}{\tau_{cs}} = \frac{u_*^2 - u_{*cs}^2}{u_{*cs}^2} \tag{5.51}$$

where τ_b is the bed stress and τ_{cs} is the critical Shields stress. The use of Smith and McLean's formulation requires that the critical Shields stress be specified for each sediment size class. Van Rijn's formula is

$$S_{eq} = 0.015 \rho_s \frac{d}{z_{eq}^*} T^{3/2} R_d^{-1/5} \tag{5.52}$$

where z_{eq}^* (= Hz_{eq}) is the dimensional reference height and R_d is a sediment grain Reynolds number. When Van Rijn's formula is select for use in EFDC, the critical Shields stress in internally calculated using relationships from Van Rijn (1984b). Van Rijn suggested setting the dimensional reference height to three grain diameters. In the EFDC model, the user specifies the reference height as a multiple of the largest noncohesive sediment size class diameter.

Garcia and Parker's general formula for multiple sediment size classes is

$$S_{jeq} = \rho_s \frac{A(\lambda Z_j)^5}{\left(1 + 3.33 A(\lambda Z)^5\right)} \tag{5.53}$$

$$Z_j = \frac{u_*}{w_{sj}} R_{dj}^{3/5} F_H \tag{5.54}$$

$$F_H = \left(\frac{d_j}{d_{50}}\right)^{1/5} \tag{5.55}$$

$$\lambda = 1 + \frac{\sigma_f}{\sigma_{fo}} (\lambda_o - 1) \tag{5.56}$$

where A is a constant equal to 1.3E-7, d_{50} is the median grain diameter based on all sediment classes, λ is a straining factor, F_H is a hiding factor and σ_f is the standard deviation of the sedimentological phi scale of sediment size distribution. Garcia and Parker's formulation is unique in that it can account for armoring effects when multiple sediment classes are simulated. For simulation of a single noncohesive size class, the straining factor and the hiding factor are set to one. The EFDC model has the option to simulate armoring with Garcia and Parker's formulation. For armoring simulation, the current surface layer of the sediment bed is restricted to a thickness equal to the dimensional reference height.

6. Cohesive Sediment Settling, Deposition and Resuspension

The settling of cohesive inorganic sediment and organic particulate material is an extremely complex process. Inherent in the process of gravitational settling is the process of flocculation, where individual cohesive sediment particles and particulate organic particles aggregate to form larger groupings or flocs having settling characteristics significantly different from those of the component particles (Burban et al., 1989,1990; Gibbs, 1985; Mehta et al., 1989). Floc formation is dependent upon the type and concentration of the suspended material, the ionic characteristics of the environment, and the fluid shear and turbulence intensity of the flow environment. Progress has been made in first principles mathematical modeling of floc formation or aggregation, and disaggregation by intense flow shear (Lick and Lick, 1988; Tsai, et al., 1987). However, the computational intensity of such approaches precludes direct simulation of flocculation in operational cohesive sediment transport models for the immediate future.

An alternative approach, which has met with reasonable success, is the parameterization of the settling velocity of flocs in terms of cohesive and organic material fundamental particle size, *d*; concentration, *S*; and flow characteristics such as vertical shear of the horizontal velocity, *du/dz*, shear stress, $A_v du/dz$, or turbulence intensity in the water column or near the sediment bed, *q*. This has allowed semi-empirical expressions having the functional form

$$W_{se} = W_{se}\left(d, S, \frac{du}{dz}, q\right) \tag{6.1}$$

to be developed to represent the effective settling velocity. A widely used empirical expression, first incorporated into a numerical by Ariathurai and Krone (1976), relates the effective settling velocity to the sediment concentration:

$$w_s = w_{so}\left(\frac{S}{S_o}\right)^a \tag{6.2}$$

with the o superscript denoting reference values. Depending upon the reference concentration and the value of α, this equation predicts either increasing or decreasing settling velocity as the sediment concentration increases. Equation (6.2) with user defined base settling velocity, concentration and exponent is an option in the EFDC model. Hwang and Metha (1989) proposed

$$w_s = \frac{aS^n}{\left(S^2 + b^2\right)^m} \tag{6.3}$$

based on observations of settling at six sites in Lake Okeechobee. This equation has a general parabolic shape with the settling velocity decreasing with decreasing concentration at low concentrations and decreasing with increasing concentration at high concentration. A least squares for the paramters, a, m, and n, in (6.3) was shown to agree well with observational data. Equation (6.3) does not hav a dependence on flow characteristics, but is based on data from an energetic field condition having both currents and high frequency surface waves. A generalized form of (6.3) can be selected as an option in the EFDC model.

Ziegler and Nisbet, (1994, 1995) proposed a formulation to express the effective settling as a function of the floc diameter, d_f

$$w_s = a d_f^b \tag{6.4}$$

with the floc diameter given by:

$$d_f = \left(\frac{\alpha_f}{S\sqrt{\tau_{xz}^2 + \tau_{xz}^2}} \right)^{1/2} \tag{6.5}$$

where S is the sediment concentration, α_f is an experimentally determined constant and τ_{xz} and τ_{yz} are the x and y components of the turbulent shear stresses at a given position in the water column. Other quantities in (6.4) have been experimentally determined to fit the relationships:

$$a = B_1 \left(S\sqrt{\tau_{xz}^2 + \tau_{xz}^2} \right)^{-0.85} \tag{6.6}$$

$$b = -0.8 - 0.5 \log\left(S\sqrt{\tau_{xz}^2 + \tau_{xz}^2} - B_2 \right) \tag{6.7}$$

where B_1 and B_2 are experimental constants. This formulation is also an option in the EFDC model.

A final settling option in EFDC is based on that proposed by Shrestha and Orlob (1996). The formulation in EFDC has the form

$$w_s = S^a \exp(-4.21 + 0.147G) \tag{6.8}$$
$$\alpha = 0.11 + 0.039G$$

where

$$G = \sqrt{(\partial_z u)^2 + (\partial_z v)^2} \tag{6.9}$$

is the magnitude of the vertical shear of the horizontal velocity. It is noted that all of these formulations are based on specific dimensional units for input parameters and predicted settling velocities and that appropriate unit conversion are made internally in their implementation in the EFDC model.

Water column-sediment bed exchange of cohesive sediments and organic solids is controlled by the near bed flow environment and the geomechanics of the deposited bed. Net deposition to the bed occurs as the flow-induced bed surface stress decreases. The most widely used expression for the depositional flux is:

$$J_o^d = \begin{cases} -w_s S_d \left(\dfrac{t_{cd} - t_b}{t_{cd}} \right) = -w_s T_d S_d \quad : \quad t_b \le t_{cd} \\ \\ 0 \quad : \quad t_b \ge t_{cd} \end{cases} \tag{6.10}$$

where t_b is the stress exerted by the flow on the bed, t_{cd} is a critical stress for deposition which depends on sediment material and floc physiochemical properties (Mehta et al., 1989) and S_d is the near bed depositing sediment concentration. The critical deposition stress is generally determined from laboratory or in situ field observations and values ranging form 0.06 to 1.1 N/m**2 have been reported in the literature. Given this wide range of reported values, in the absence of site specific data the depositional stress and is generally treated as a calibration parameter. The depositional stress is an input parameter in the EFDC model.

Since the near bed depositing sediment concentration in (6.10) is not directly calculated, the procedures of Chapter 5 can be applied to relate the the near bed depositional concentration to the bottom layer or depth averge concentration. Using (5.14) the near bed concentration during times of deposition can be determined in terms of the bottom layer concentration for three-dimensional model applications. Inserting (6.10) into (5.14) and evaluating the constant at a near bed depositional level gives

$$S = \left(T_d + (1 - T_d) \frac{z_d^R}{z^R} \right) S_d \tag{6.11}$$

Integrating (6.11) over the bottom layer gives

$$\begin{aligned} S_d &= \left(T_d + \frac{\ln\left(\Delta z_d^{-1}\right)}{\left(\Delta z_d^{-1} - 1\right)} (1 - T_d) \right)^{-1} \bar{S} : R = 1 \\ S_d &= \left(T_d + \frac{\left(\left(\Delta z_{eq}^{-1}\right)^{1-R} - 1 \right)}{(1-R)\left(\Delta z_d^{-1} - 1\right)} (1 - T_d) \right)^{-1} \bar{S} : R \ne 1 \end{aligned} \tag{6.12}$$

The corresponding quantities in the numerical solution bottom boundary condition (3.6) are

$$\begin{aligned} P_d w_s &= \left(T_d + \frac{\ln\left(\Delta z_d^{-1}\right)}{\left(\Delta z_d^{-1} - 1\right)} (1 - T_d) \right)^{-1} w_s : R = 1 \\ P_d w_s &= \left(T_d + \frac{\left(\left(\Delta z_{eq}^{-1}\right)^{1-R} - 1 \right)}{(1-R)\left(\Delta z_d^{-1} - 1\right)} (1 - T_d) \right)^{-1} w_s : R \ne 1 \end{aligned} \tag{6.13}$$

For depth averaged model application, (6.10) is combined with (5.25) and the constant of integration is evaluated at a near bed depositional level to give

$$S = \left(1 - \frac{Rz}{(1+R)}\right) T_d S_d + \left(1 - \left(1 - \frac{Rz_d}{(1+R)}\right) T_d\right) S_d \frac{z_d^R}{z^R} \tag{6.14}$$

Integrating (6.14) over the depth gives

$$S_d = \left(\left(\frac{2 + R(1 - z_d)}{2(1+R)}\right) T_d + \frac{\ln\left(z_d^{-1}\right)}{\left(z_d^{-1} - 1\right)}\left(1 - \left(\frac{1 + R(1 - z_d)}{(1+R)}\right) T_d\right)\right)^{-1} \bar{S} : R = 1$$

$$S_d = \left(\left(\frac{2 + R(1 - z_d)}{2(1+R)}\right) T_d + \frac{\left(z_d^{R-1} - 1\right)}{(1-R)\left(z_d^{-1} - 1\right)}\left(1 - \left(1 - \frac{Rz_d}{(1+R)}\right) T_d\right)\right)^{-1} \bar{S} : R \neq 1 \tag{6.15}$$

The corresponding quantities in the numerical solution bottom boundary condition (3.6) are

$$P_d w_s = \left(\left(\frac{2 + R(1 - z_d)}{2(1+R)}\right) T_d + \frac{\ln\left(z_d^{-1}\right)}{\left(z_d^{-1} - 1\right)}\left(1 - \left(\frac{1 + R(1 - z_d)}{(1+R)}\right) T_d\right)\right)^{-1} w_s : R = 1$$

$$P_d w_s = \left(\left(\frac{2 + R(1 - z_d)}{2(1+R)}\right) T_d + \frac{\left(z_d^{R-1} - 1\right)}{(1-R)\left(z_d^{-1} - 1\right)}\left(1 - \left(1 - \frac{Rz_d}{(1+R)}\right) T_d\right)\right)^{-1} w_s : R \neq 1 \tag{6.16}$$

It is noted that the assumptions used to arrive at the relationships, (6.12) and (6.15) are more teneous for cohesive sediment than the similar relationships for noncohesive sediment. The settling velocity for cohesive sediment is highly concentration dependent and the use of a constant settling velocity to arrive at (6.12) and (6.15) is questionable. The specification of an appropriate reference level for cohesive sediment is difficult. One possibility is to relate the reference level to the floc diameter using (6.5). An alternative is to set the reference level to a laminar sublayer thickness

$$z_d = \frac{\nu(S)}{Hu_*} \tag{6.17}$$

where $\nu(S)$ is a sediment concentration dependent kinematic viscosity and the water depth is include to nondimensionlize the reference level. A number of investigators, including Mehta and Jiang (1990) have presented experimental results indicating that at high sediment concentrations, cohesive sediment-water mixtures behave as high viscosity fluids. Mehta and Jain's results indicate that a sediment concentration of 10,000 mg/L results in a viscosity ten time that of pure water and that the viscosity increases logrithmically with increasing mixture density. Use of the relationships (6.12) and (6.16) is optional in the EFDC model. When they are used, the reference height is set using (6.17) with the viscosity determined using Mehta and Jain's experimental relationship between viscosity and sediment concentration. To more fully address the deposition prediction problem, a nested sediment, current and wave boundary layer model based on the near bed closure presented in Chapter 4 is under development.

Cohesive bed erosion occurs in two distinct modes, mass erosion and surface erosion. Mass erosion occurs rapidly when the bed stress exerted by the flow exceeds the depth varying shear strength, τ_s, of the bed at a depth, H_{me}, below the bed surface. Surface erosion occurs gradually when the flow-exerted bed stress is less than the bed shear strength near the surface but greater than a critical erosion or resuspension stress, τ_{ce}, which is dependent on the shear strength and density of the bed. A typical scenario under conditions of accelerating flow and increasing bed stress would involve first the occurrence of gradual surface erosion, followed by a rapid interval of mass erosion, followed by another interval of surface erosion. Alternately, if the bed is well consolidated with a sufficiently high shear strength profile, only gradual surface erosion would occur. Transport into the water column by mass or bulk erosion can be expressed in the form

$$J_o^r = w_r S_r = \frac{m_{me}(\tau_s \le \tau_b)}{T_{me}} \tag{6.18}$$

where J_o is the erosion flux, the product $w_r S_r$ represents the numerical boundary condition (3.6), m_{me} is the dry sediment mass per unit area of the bed having a shear strength, τ_s, less than the flow-induced bed stress, τ_b, and T_{me} is a somewhat arbitrary time scale for the bulk mass transfer. The time scale can be taken as the numerical model integration time step (Shrestha and Orlob, 1996). Observations by Hwang and Mehta (1989) have indicated that the maximum rate of mass erosion is on the order of 0.6 gm/s-m**2 which provides an means of estimating the transfer time scale in (4.10). The shear strenght of the cohesive sediment bed is generally agreed to be a linear function of the bed bulk density (Metha et al., 1982; Villaret and Paulic, 1986; Hwang and Mehta, 1989)

$$\tau_s = a_s \rho_b + b_s \tag{6.19}$$

For the shear strength in N/m**2 and the bulk density in gm/cm**3, Hwang and Mehta (1989) give a_s and b_s values of 9.808 and -9.934 for bulk density greater than 1.065 gm/cm**3. The EFDC model currently implements Hwang and Mehta's relationship, but can be readily modified to incorporated other functional relationships.

Surface erosion is generally represented by relationships of the form

$$J_o^r = w_r S_r = \frac{dm_e}{dt}\left(\frac{\tau_b - \tau_{ce}}{\tau_{ce}}\right)^a \quad : \quad \tau_b \ge \tau_{ce} \tag{6.20}$$

or

$$J_o^r = w_r S_r = \frac{dm_e}{dt}\exp\left(-\beta\left(\frac{\tau_b - \tau_{ce}}{\tau_{ce}}\right)^\gamma\right) \quad : \quad \tau_b \ge \tau_{ce} \tag{6.21}$$

where dm_e/dt is the surface erosion rate per unit surface area of the bed and τ_{ce} is the critical stress for surface erosion or resuspension. The critical erosion rate and stress and the parameters α, β, and γ are generally determined from laboratory or in situ field experimental observations.

Equation (6.20) is more appropriate for consolidated beds, while (6.21) is appropriate for soft partially consolidated beds. The base erosion rate and the critical stress for erosion depend upon the type of sediment, the bed water content, total salt content, ionic species in the water, pH and temperature (Mehta, *et al*., 1989) and can be measured in laboratory and sea bed flumes.

The critical erosion stress is related to but generally less than the shear strength of the bed, which in turn depends upon the sediment type and the state of consolidation of the bed. Experimentally determined relationships between the critical surface erosion stress and the dry density of the bed of the form

$$\tau_{ce} = c\,\rho_s^d \tag{6.22}$$

have been presented (Mehta, et al., 1989). Hwang and Mehta (1989) proposed the relationship

$$\tau_{ce} = a\left(\rho_b - \rho_l\right)^b + c \tag{6.23}$$

between the critical surface erosion stress and the bed bulk density with a, b, c, and ρ_l equal to 0.883, 0.2, 0.05, and 1.065, respectively for the stress in N/m**2 and the bulk density in gm/cm**3. Considering the relationship between dry and bulk density

$$\rho_d = \rho_s \frac{\left(\rho_b - \rho_w\right)}{\left(\rho_s - \rho_w\right)} \tag{6.24}$$

equations (6.22) and (6.23) are consistent. The EFDC model allow for a user defined constant critial stress for surface erosion or the use of (6.23). Alternate predictive expression can be readily incorporated into the model.

Surface erosion rates ranging from 0.005 to 0.1 gm/s-m**2 have been reported in the literature, and it is generally accepted that the surface erosion rate decreases with increasing bulk density. Based on experimental observations, Hwang and Mehta (1989) proposed the relationship

$$\log_{10}\left(\frac{dm_e}{dt}\right) = 0.23\exp\left(\frac{0.198}{\rho_b - 1.0023}\right) \tag{6.25}$$

for the erosion rate in mg/hr-cm**2 and the bulk density in gm/cm**3. The EFDC model allow for a user defined constant surface erosion rate or predicts the rate using (6.25). Alternate predictive expression can be readily incorporated into the model. The use of bulk density functions to predict bed strength and erosion rates in turn requires the prediction of time and depth in bed variations in bulk density which is related to the water and sediment density and the bed void ratio by

$$\rho_b = \left(\frac{e}{1+e}\right)\rho_w + \left(\frac{1}{1+e}\right)\rho_s \tag{6.26}$$

Selection of the bulk density dependent formulations in the EFDC model requires implmentation of a bed consolidation simulation to predict the bed void ratio as discussed in the following chapter.

7. Sediment Bed Geomechanical Processes

This chapter describes the representation of the sediment bed in the EFDC model. To make the information presented self contained, the derivation of mass balance equations and comparison with formulations used in other models is also presented.

Consider a sediment bed represented by discrete layers of thickness B_k, which may be time varying. The conservation of sediment and water mass per unit horizontal area in layer k is given by:

$$\P_t\left(\frac{\rho_s B_k}{1+\varepsilon_k}\right) = J_{s:k-} - J_{s:k+} - \delta(k,k_b) J_{sb} \tag{7.1}$$

$$\P_t\left(\frac{\rho_w \varepsilon_k B_k}{1+\varepsilon_k}\right) = J_{w:k-} - J_{w:k+} - \delta(k,k_b)\frac{\rho_w}{\rho_s}\left(\varepsilon_k \max(J_{sb},0) + \varepsilon_b \min(J_{sb},0)\right) \tag{7.2}$$

where ε is the void ratio, ρ_s and ρ_w are the sediment and water density and J_s and J_w are the sediment and water mass fluxes with $k-$ and $k+$ defining the bottom and top boundaries, respectively of layer k. The mass fluxes are defined as positive in the vertical direction and exclude fluxes associated with sediment depostion and erosion. The last term in equation (7.1) represents erosion and deposition of sediment at the top of the upper most bed layer, $k=k_b$, where

$$\delta(k,k_b) = \begin{cases} 1 : k = k_b \\ 0 : k \neq k_b \end{cases} \tag{7.3}$$

Consitent with this partitioning of flux,

$$J_{s:k+} = 0 : k \neq k_b \tag{7.4}$$

The last term in (7.2) represents the corresponding entrainment of bed water into the water column during sediment erosion and entrainment of water column water into the bed during deposition. The water flux, $J_{w:k+}$, at the top of the upper most layer, k_b, is not necessarily zero, since it can include ambient seepage and pore water explusion due to bed consolidation.

Assuming sediment and water to be incompressible, (7.1) and (7.2) can be written as:

$$\P_t\left(\frac{B_k}{1+\varepsilon_k}\right) = \frac{1}{\rho_s}\left(J_{s:k-} - J_{s:k+}\right) - \delta(k,k_b)\frac{J_{sb}}{\rho_s} \tag{7.5}$$

$$\partial_t\left(\frac{\varepsilon_k B_k}{1+\varepsilon_k}\right) = q_{w:k-} - q_{w:k+} - \delta(k,k_b)\left(\varepsilon_k \max\left(\frac{J_{sb}}{\rho_s},0\right) + \varepsilon_b \min\left(\frac{J_{sb}}{\rho_s},0\right)\right) \tag{7.6}$$

where the water specfic discharges

$$\begin{aligned} J_{w:k-} &= \rho_w q_{w:k-} \\ J_{w:k+} &= \rho_w q_{w:k-} \end{aligned} \tag{7.7}$$

have been introduced into (7.6). Four approaches for the solution of the mass conservation equations (7.5) and (7.6) have been previously utilized. The solution approaches, hereafter referred to as solution levels, increase in complexity and physical realism and will be briefly summarized.

The first level or simplest approach assumes specified time-constant layer thicknesses and void ratios with the left sides of (7.5) and (7.6) being identically zero. Sediment mass flux at all layer interfaces are then identical to the net flux from the bed to the water column.

$$\begin{aligned} J_{s:k-} &= J_{sb} : k = 1, k_b \\ J_{s:k+} &= \begin{cases} 0 : k = k_b \\ J_{sb} : k \neq k_b \end{cases} \end{aligned} \tag{7.8}$$

Bed representations at this level, as exemplified by the RECOVERY model (Boyer, et al., 1994), typically omit the water mass conservation equations. However, it is noted that the water mass conservation is ill posed unless either q_{1-}, the specific discharge at the bottom of the deepest layer or q_{kb+}, the specific discharge at the top of the water column adjacent layer, is specified. If q_{1-} is set to zero, q_{ka+} is then required to exactly cancel the entrainment terms is (7.6).

The second level of bed mass conservation representation assumes specified time invariant layer thicknesses. The mass conservation equations (7.5) and (7.6) become

$$B_k \partial_t\left(\frac{1}{1+\varepsilon_k}\right) = \frac{1}{\rho_s}\left(J_{s:k-} - J_{s:k+}\right) - \delta(k,k_b)\frac{J_{sb}}{\rho_s} \tag{7.9}$$

$$B_k \partial_t\left(\frac{\varepsilon_k}{1+\varepsilon_k}\right) = q_{w:k-} - q_{w:k+} - \delta(k,k_b)\left(\varepsilon_k \max\left(\frac{J_{sb}}{\rho_s},0\right) + \varepsilon_b \min\left(\frac{J_{sb}}{\rho_s},0\right)\right) \tag{7.10}$$

This system of 2 x k_b equations includes k_b unknow void ratios, k_b unknow internal sediment fluxes, and k_{b+1} unknow specific discharges and is under determined unless additional information is specified. The constant bed layer thickness option in the WASP5 model (Ambrose, et al., 1993) uses specifed burial velocities to define the internal sediment fluxes

$$J_{s:k-} = -w_{b:k-} S_k$$
$$J_{s:k+} = -w_{b:k+} S_{k+1} \qquad (7.11)$$
$$w_{b:k+} = w_{b:k+1-}$$

$$S_k = \frac{\rho_s}{1+\varepsilon_k} \qquad (7.12)$$

where w_b is the burial velocity and S is the sediment concentration (mass per unit total volume). Use of the burial velocity eliminates the indeterminacy in (7.9) and allowing its solution for the void ratio. In the event that the sediment concentration in the upper most layer becomes negative, the layer is eliminated and the underlying layer become water column adjacent. The left side of the water mass conservation equations (7.10) is now know and the equation is more appropriately written as

$$q_{w:k-} - q_{w:k+} = B_k \partial_t \left(\frac{\varepsilon_k}{1+\varepsilon_k} \right) + \delta(k, k_b) \left(\varepsilon_k \max\left(\frac{J_{sb}}{\rho_s}, 0 \right) + \varepsilon_b \min\left(\frac{J_{sb}}{\rho_s}, 0 \right) \right) \qquad (7.13)$$

The determination of the specific discharges using (7.13) can be viewed is either under determined or physically inconsistent. As shown for the first level approach, the solution of (7.13) is ill posed unless either q_{1-}, the specific discharge at the bottom of the deepest layer or q_{kb+}, the specific discharge at the top of the upper most layer is independently specified. If q_{1-} is specified and the internal specific discharges are determined from (7.13), q_{ka+} is then required to partially cancel the entrainment terms in (7.13). As will be subsequently shown, the specific discharges can be dynamically determined using Darcy's law. However, the specific discharges determined using Darcy's law and the known void ratios are not guaranteed to satisfy (7.13) the level two formulation is dynamically inconsistent with respect to water mass conservation in the sediment bed. The constant bed layer thickness option in the WASP5 ignores this problem entirely by not considering the water mass balance and hence neglecting pore water advection of dissolved contaminants.

The third level of bed mass conservation representation assumes specified time invariant layer void ratios. The mass conservation equations (7.5) and (7.6) become

$$\left(\frac{1}{1+\varepsilon_k} \right) \partial_t B_k = \frac{1}{\rho_s} \left(J_{s:k-} - J_{s:k+} \right) - \delta(k, k_b) \frac{J_{sb}}{\rho_s} \qquad (7.14)$$

$$\left(\frac{\varepsilon_k}{1+\varepsilon_k} \right) \partial_t B_k = q_{w:k-} - q_{w:k+} - \delta(k, k_b) \left(\varepsilon_k \max\left(\frac{J_{sb}}{\rho_s}, 0 \right) + \varepsilon_b \min\left(\frac{J_{sb}}{\rho_s}, 0 \right) \right) \qquad (7.15)$$

This system of equations exhibits the same under determined nature as (7.9) and (7.10). Specification of internal sediment fluxes or burial velocities allows (7.14) to be solved for the layer thicknesses. Solution of (7.15) for the specific discharges then requires the specification either q_{1-}, the specific discharge at the bottom of the deepest layer or q_{kb+}, the specific discharge at the top of the upper most layer. The variable bed layer thickness option in the WASP5 model

(Ambrose, et al., 1993) exemplifies the third level of bed representation. Specifically, the thickness of the water column adjacent layer is allowed to vary in time, while the thicknesses of the underlying layers remain constant. A periodic time variation is specified for the bottom sediment flux in the upper most layer

$$J_{s:kb-} = 0 \quad : \quad t_o \le t \le t_o + (N-1)\Delta t$$
$$J_{s:kb-} = \int_{t_o}^{t_o + N\Delta t} J_{sb}\, dt \quad : \quad t_o + (N-1)\Delta t \le t \le t_o + N\Delta t \qquad (7.16)$$

where Δt is the standard water time step and $N\Delta t$ is the sediment compaction time. This results in the thickness of the upper most layer periodically returning to its initial value at time intervals of $N\Delta t$ unless the thickness becomes negative due to net resuspension. In that event, the underlying layer becomes the water column adjacent layer. The water mass conservation (7.15) for all but the upper most layer becomes

$$q_{k+} = q_{k-} = q_{1-} \quad : \quad k \ne k_b \qquad (7.17)$$

indicating that all internal specific discharges are equal a specified specific discharge at the bottom of layer 1. Given the solution for the time variation of the water column adjacent thickness and bottom specific discharge, (7.15) can be solved for the specific discharge at the top of the layer. The constant porosity bed option in EFDC is also a level three approach. In EFDC, the internal sediment fluxes are set to zero and the change in thickness of the water column adjacent layer is determined directly using (7.14) while the underlying layers have time invariant thicknesses. As a result, the internal water specific discharges are set to zero and the water entrainment and expulsion in the water column adjacent layer are determined directly from (7.15). The EFDC model is configured to have a user specified maximum number of sediment bed layer. A the start of a simulation, the number of layers containing sediment at a specific horizontal location is specified. Under continued deposition, a new water column layer is created when the thickness of the current layer exceeds a user specified value. If the current water column adjacent layer's index is equal to the maximam number of layers, the bottom two layers are combined and the remaining layers renumbered before addition of the new layer. Under continued resuspension, the layer underlying the current water column adjacent layer becomes the new adjacent layer when all sediment is resuspended form the current layer.

The fourth level of bed representation accounts for bed consolidation by allowing the layer void ratios and thicknesses to vary in time. The simplest and most elegant formulations at this level utilize a Lagrangian approach for sediment mass conservation. The Lagrangian approach requires that the sediment mass per unit horizontal area in all layers, except the upper most, be time invariant and without loss of generality, the internal sediment fluxes can be set to zero. Consistent with these requirements (7.5) becomes

$$\partial_t \left(\frac{B_k}{1+\varepsilon_k} \right) = -\delta(k,k_b) \frac{J_{sb}}{\rho_s} \qquad (7.18)$$

Expanding the left side of the water conservation equation (7.6), and using (7.18) gives

$$\left(\frac{B_k}{1+\varepsilon_k}\right)\partial_t \varepsilon_k = q_{w:k-} - q_{w:k+} + \delta(k,k_b)(\varepsilon_k - \varepsilon_b)\min\left(\frac{J_{sb}}{\tau_s}, 0\right) \tag{7.19}$$

The Lagrangian approach for sediment mass conservation also requires that the number of bed layers vary in time. Under conditions of continued deposition, a new water column adjacent layer would be added when either the thickness, void ratio or mass per unit area of the current water column adjacent layer reaches a predefined value. Under conditions of continued resuspension, the bed layer immediately under the current water column adjacent layer would become the new water column adjacent layer when the entire sediment mass of the current layer has been resuspended.

At the fourth and most realistic level of bed representation, three approaches can be used to represent bed consolidation. Two of the approaches are semi-empirical with the first assuming that the void ratio of a layer decreases with time. A typical relationship which is used for the simple consolidation option in the EFDC model is

$$\varepsilon = \varepsilon_m + (\varepsilon_o - \varepsilon_m)\exp(-\alpha(t - t_o)) \tag{7.20}$$

where ε_o is the void ratio at the mean time of deposition, t_o, ε_m is the ultimate minimum void ratio corresponding to complete consolidation, and α is an empirical or experimental constant. Use of (7.20) in the EFDC model involves specifying the depositional void ratio, the ultimate void ratios and the rate constants. The ultimate void ratio can be specified as a function depth below the water column-bed interface. The actual calculation involves using the initial void ratios to determine the deposition time t_o, after which (7.20) is used to update the void ratios as the simulation progresses. After equation (7.20) is used to calculate the new time level void ratios, equation (7.18) provides the new layer thicknesses. The water conservation equations (7.19) can then be solved using

$$q_{w:k+} = q_{w:k-} - \left(\frac{B_k}{1+\varepsilon_k}\right)\partial_t \varepsilon_k + \delta(k,k_b)(\varepsilon_k - \varepsilon_b)\min\left(\frac{J_{sb}}{\tau_s}, 0\right) \tag{7.21}$$

to determine the water specific discharges, provided that the specific discharge q_{1-}, at the bottom of layer *1* is specified. When this option is specified in the EFDC model, the specific discharge at bottom of the bottom sediment layer is set to zero. Layers are added and deleted in the manner previously described for EFDC's constant porosity option. The SED2D-WES model (Letter et al., 1998) utilizes a similar approach based on a specified time variation of bulk density

$$\rho_b = \frac{\rho_s + \varepsilon\rho_w}{1+\varepsilon} = \rho_{bm} + (\rho_{bo} - \rho_{bm})\exp(-\alpha(t - t_o)) \tag{7.22}$$

which in turn defines the variation in void ratio.

The second semi-empirical approach assumes that the vertical distribution of the bed bulk density or equivalently the, void ratio at any time is given by a self-similar function of vertical position, bed thickness and fixed surface and bottom bulk densities or void ratios. Functionally this equivalent to

$$\varepsilon = V(z, B_T, \varepsilon_{kb}, \varepsilon_1) \tag{7.23}$$

where V represents the function, z is a vertical coordinate measured upward from the bottom of the lowest layer, and B_T is the total thickness of the bed. This approach is used in the original HSTM model (Hayter and Mehta, 1983), the new HSCTM model (Hayter et al., 1998) and is an option in the CE-QUAL-ICM/TOXI model (Dortch, et al., 1998). The determination of the new time level layer thicknesses and void ratios requires an iterative solution of equations (7.18) and (7.23). The solution is completed using (7.21) to determine the water specific discharges.

The third and most realistic approach is to dynamically simulate the consolidation of the bed. In the Lagrangian formulation, (7.18) is directly solved for the equivalent sediment thickness

$$\Delta_k = \frac{B_k}{1+\varepsilon_k} \tag{7.24}$$

and the water conservation equation (7.19) is integrated to determine the void ratio.

$$\Delta_k \partial_t \varepsilon_k = q_{w:k-} - q_{w:k+} + \delta(k, k_b)(\varepsilon_k - \varepsilon_b)\min\left(\frac{J_{sb}}{\rho_s}, 0\right) \tag{7.25}$$

The specific discharges in (7.25) are determined using the Darcy equation

$$q = -\frac{K}{g\rho_w}\partial_z u \tag{7.26}$$

where K is the hydraulic conductivity and u is the excess pore pressure defined as the difference between the total pore pressure u_t, and the hydrostatic pressure u_h.

$$u = u_t - u_h \tag{7.27}$$

The total pore pressure is defined as the difference between the total stress σ and effective stress σ_e.

$$u_t = \sigma - \sigma_e \tag{7.28}$$

The total stress and hydrostatic pressure are given by

$$\sigma = p_b + g\int_z^{z_b}\left(\left(\frac{\varepsilon}{1+\varepsilon}\right)\rho_w + \left(\frac{1}{1+\varepsilon}\right)\rho_s\right)dz \tag{7.29}$$

$$u_h = p_b + g\rho_w(z_b - z) \tag{7.30}$$

where p_b is the water column pressure at the bed z_b. Solving for the excess pore pressure using (7.27) through (7.30) gives

$$u = g\rho_w\left(\frac{\rho_s}{\rho_w} - 1\right)\int_z^{z_b}\left(\frac{1}{1+e}\right)dz - \sigma_e \tag{7.31}$$

The specific discharge (7.26), can alternately be expressed in terms of the effective stress

$$q = \frac{K}{g\rho_w}\nabla_z\sigma_e - \left(\frac{\rho_s}{\rho_w} - 1\right)K\nabla_z\left(\int_z^{z_b}\left(\frac{1}{1+e}\right)dz\right) \tag{7.32}$$

or the void ratio

$$q = \frac{K}{g\rho_w}\left(\frac{d\sigma_e}{de}\right)\nabla_z e - \left(\frac{\rho_s}{\rho_w} - 1\right)K\nabla_z\left(\int_z^{z_b}\left(\frac{1}{1+e}\right)dz\right) \tag{7.33}$$

where $de/d\sigma_c$ is a coefficient of compressibility.

For consistency with the Lagrangian representation of sediment mass conservation, a new vertical coordinate ζ, defined by

$$\frac{d\zeta}{dz} = \frac{1}{1+e} \tag{7.34}$$

is introduced. The discrete form of (7.34) is

$$\zeta_{k+} - \zeta_{k-} = \frac{z_{k+} - z_{k-}}{1+e_k} = \frac{B_k}{1+e_k} = \Delta_k \tag{7.35}$$

where D is the equivalent sediment thickness previously defined by (7.24). Introducing (7.34) into (7.26), (7.32), and (7.33) gives

$$q = -\frac{K}{g\rho_w(1+e)}\nabla_z u \tag{7.36}$$

$$q = \frac{K}{g\rho_w(1+e)}\nabla_z\sigma_e + \left(\frac{\rho_s}{\rho_w} - 1\right)\frac{K}{(1+e)} \tag{7.37}$$

$$q = \lambda\left(\frac{K}{1+e}\right)\nabla_z e + \left(\frac{\rho_s}{\rho_w} - 1\right)\left(\frac{K}{1+e}\right) \tag{7.38}$$

where

$$\lambda = \frac{1}{g\rho_w}\frac{d\sigma_e}{de} \tag{7.39}$$

is a compressibility length.

Three formulations for the solution the consolidation problem can be utilized. The void ratio-excess pore pressure formulation, used in the EFDC model, evaluates the specific discharges at the current time level *n*, using (7.36) and explicitly integrates (7.25)

$$e_k^{n+1} = e_k^n + \frac{q}{\Delta_k^n}\left(q_{w:k-} - q_{w:k+} + d(k,k_b)(e_k - e_b)\min\left(\frac{J_{sb}}{r_s},0\right)\right)^n \tag{7.40}$$

where q is the time step, to give the new time level void ratios. The layer thicknesses are then determined by explicit integration of (7.18).

$$\left(\frac{B}{1+e}\right)_k^{n+1} = \left(\frac{B}{1+e}\right)_k^n - qd(k,k_b)\frac{J_{sb}}{r_s}$$
$$\Delta_k^{n+1} = \Delta_k^n - qd(k,k_b)\frac{J_{sb}}{r_s} \tag{7.41}$$

Constitutive equations required for consolidation prediction generally express the effective stress and hydraulic conductivity as functions of the void ratio. Thus the new time level void ratio is used to determine new time level values of the effective stress and hydraulic conductivity. The new time level excess pore pressures is then given by

$$u = gr_w\left(\frac{r_s}{r_w} - 1\right)(z_b - z) - s_e \tag{7.42}$$

the transformed equivalent of (7.31). The primary advantage of the void ratio-excess pore pressure formulation is the simplicity of its boundary conditions

$$u = u_b : z = z_b \tag{7.43}$$

$$u = u_o : z = 0$$
$$or$$
$$q = q_o : z = 0 \tag{7.44}$$

The water column-sediment bed interface boundary condition generally sets u_b to zero if the surface water flow is hydrostatic but can incorporate wave induced pore pressures. The bottom boundary conditions allows either the specification of pressure or specific discharge. The primary disadvantage of this formulation is the stability or positivity criterion imposed on the time step

$$q \le \frac{\Delta_k^n e_k^n}{\left(q_{w:k+} - q_{w:k-} + d(k,k_b)(e_b - e_k)\min\left(\frac{J_{sb}}{r_s},0\right)\right)^n} \tag{7.40}$$

$$\theta \le \frac{\Delta_k^n}{\delta(k,k_b)\max\left(\frac{J_{sb}}{\rho_s},0\right)} \tag{7.41}$$

In practice, these criteria are readily satisfied if the consolidation time step is identical to the time step of the hydrodynamic model. In the event that these criteria are not met using the hydrodynamic time step, the bed consolidation is sub-cycled using an integer number of time steps, meeting (7.40) and (7.41), per each hydrodynamic time step.

Alternately, the consolidation problem can be directly formulated in terms of the effective stress or void ratio. Combining (7.25) and (7.37) using (7.39) gives the effective stress formulation

$$\Delta_k \partial_t \varepsilon_k = \left(\lambda\left(\frac{K}{1+\varepsilon}\right)\partial_z \varepsilon + \left(\frac{\rho_s}{\rho_w}-1\right)\left(\frac{K}{1+\varepsilon}\right)\right)_{k-}$$
$$-\left(\lambda\left(\frac{K}{1+\varepsilon}\right)\partial_z \varepsilon + \left(\frac{\rho_s}{\rho_w}-1\right)\left(\frac{K}{1+\varepsilon}\right)\right)_{k+} + \delta(k,k_b)(\varepsilon_k-\varepsilon_b)\min\left(\frac{J_{sb}}{\rho_s},0\right) \tag{7.42}$$

The continuum equivalent is

$$\frac{1}{\lambda}\partial_t \sigma_{e:k} = -\partial_z\left(\frac{K}{(1+\varepsilon)}\partial_z \sigma_e + g(\rho_s-\rho_w)\frac{K}{(1+\varepsilon)}\right)$$
$$+g\rho_w\delta(\zeta_b)(\varepsilon_k-\varepsilon_b)\min\left(\frac{J_{sb}}{\rho_s},0\right) \tag{7.43}$$

which is parabolic since λ is negative. Combining (7.25) and (7.38) using (7.39) gives the void ration formulation

$$\Delta_k \partial_t \varepsilon_k = \left(\lambda\left(\frac{K}{1+\varepsilon}\right)\partial_z \varepsilon + \left(\frac{\rho_s}{\rho_w}-1\right)\left(\frac{K}{1+\varepsilon}\right)\right)_{k-}$$
$$-\left(\lambda\left(\frac{K}{1+\varepsilon}\right)\partial_z \varepsilon + \left(\frac{\rho_s}{\rho_w}-1\right)\left(\frac{K}{1+\varepsilon}\right)\right)_{k+} + \delta(k,k_b)(\varepsilon_k-\varepsilon_b)\min\left(\frac{J_{sb}}{\rho_s},0\right) \tag{7.44}$$

The continuum equivalent is

$$\partial_t \varepsilon_k = -\partial_z\left(\lambda\left(\frac{K}{1+\varepsilon}\right)\partial_z \varepsilon + \left(\frac{\rho_s}{\rho_w}-1\right)\left(\frac{K}{1+\varepsilon}\right)\right) + \delta(\zeta_b)(\varepsilon_k-\varepsilon_b)\min\left(\frac{J_{sb}}{\rho_s},0\right) \tag{7.45}$$

Equation (7.45) is the discrete form of the finite strain consolidation equation first derived by Gibson et al. (1967). Equation (7.45) was used by Cargill (1985) in the formulation of a model for dredge material consolidation and by Le Normant (1998) to represent bed consolidation in a three-dimensional cohesive sediment transport model.

The classic linear consolidation equation (Middleton and Wilcock, 1994) omits the second term associated with self weight in (7.45) and introduces a constant consolidation coefficient

$$C_c = -(1+e)\frac{\partial \sigma_e}{\partial e}\frac{K}{g\rho_w} \tag{7.46}$$

reducing (7.45) to

$$\partial_t e = C_c \partial_{zz} e \tag{7.47}$$

Equation (7.47) has separable solutions of the form

$$\begin{aligned} e &= f_n(z)\exp\left(-\lambda_n \frac{C_c}{B^2} t\right) \\ \partial_{zz} f_n &+ \lambda_n f_n = 0 \\ z &= \frac{z}{B} \end{aligned} \tag{7.48}$$

which provides some justification for empirical relationship (7.20).

The solution of the finite strain consolidation problem in any of its three forms requires constitutive relationships

$$\sigma_e = \sigma_e(e) \tag{7.49}$$

$$K = K(e) \tag{7.50}$$

Bear (1979) notes that curve fitting of experimental data typically results in relationships of the form

$$e - e_o = -a_v(\sigma_e - \sigma_{eo}) \tag{7.51}$$

$$e - e_o = -C_c \ln\left(\frac{\sigma_e}{\sigma_{eo}}\right) \tag{7.52}$$

for noncohesive and coheasive soils respectively, where a_v is the coefficient of compressibility and C_c is the compression index. Graphical presentation of experimental forms of (7.49) and (7.50) are presented in Cargill (1985) and Palermo et al., (1998) which are generally consistent with (7.52) and suggest

$$e - e_o \propto \ln\left(\frac{K}{K_o}\right) \tag{7.53}$$

as a candidate relationship between the void ratio and hydraulic conductivity for cohesive sediment beds. Similarly, a linear relationship

$$\varepsilon - \varepsilon_o \propto K - K_o \qquad (7.54)$$

would likely suffice for noncohesive sediment beds.

8. References

Ackers, P., and W. R. White, 1973: Sediment transport: New approaches and analysis. *J. Hyd. Div. ASCE*, **99**, 2041-2060.

Ariathurai, R., and R. B. Krone, 1976: Finite element model for cohesive sediment transport. *J. Hyd. Div. ASCE*, **102**, 323-338.

Ambrose, R. B., T. A. Wool, and J. L. Martin, 1993: The water quality analysis and simulation program, WASP5: Part A, model documentation version 5.1. U. S. EPA, Athens Environmental Research Laboratory, 210 pp.

Bear, J., 1879: *Hydraulics of groundwater*, McGraw-Hill, New York.

Bagnold, R. A., 1956: The flow of cohesionless grains in fluids. *Phil. Trans. Roy. Soc. Lond.,* Series A, Vol **249**, No. 964, 235-297.

Blumberg, A. F., B. Galperin, and D. J. O'Connor, 1992: Modeling vertical structure of open-channel flow. *J. Hydr. Engr.*, **118**, 1119-1134.

Boyer, J. M., S. C. Chapra, C. E. Ruiz, and M. S. Dortch, 1994: RECOVERY, a mathematical model to predict the temporal response of surface water to contaminated sediment. Tech. Rpt. W-94-4, U. S. Army Engineer Waterways Experiment Station, Vicksburg, MS, 61 pp.

Burban, P. Y., W. Lick, and J. Lick, 1989: The flocculation of fine-grained sediments in estuarine waters. *J. Geophys. Res.*, **94**, 8323-8330.

Burban, P. Y., Y. J. Xu, J. McNeil, and W. Lick, 1990: Settling speeds of flocs in fresh and seawater. *J. Geophys. Res.*, **95**, 18,213-18,220.

Cargill, K. W., 1985: Mathematical model of the consolidation and desiccation processes in dredge material. U.S. Army Corps of Engineers, Waterways Experiment Station, Technical Report D-85-4.

Dortch, M., C. Ruiz, T. Gerald, and R. Hall, 1998: Three-dimensional contaminant transport/fate model. *Estuarine and Coastal Modeling, Proceedings of the 5nd International Conference*, M. L. Spaulding and A. F. Blumberg, Eds., American Society of Civil Engineers, New York, 75-89.

Einstein, H. A., 1950: The bed load function for sediment transport in open channel flows. *U.S. Dept. Agric. Tech. Bull.*, 1026.

Galperin, B., L. H. Kantha, S. Hassid, and A. Rosati, 1988: A quasi-equilibrium turbulent energy model for geophysical flows. *J. Atmos. Sci.,* **45**, 55-62.

Garcia, M., and G. Parker, 1991: Entrainment of bed sediment into suspension. *J. Hyd. Engrg.*, **117**, 414-435.

Gibbs, R. J., 1985: Estuarine Flocs: their size, settling velocity and density. *J. Geophys. Res.*, **90**, 3249-3251.

Gibson, R. E., G. L. England, and M. J. L. Hussey, 1967: The theory of one-dimensional consolidation of saturated clays. *Geotechnique*, **17**, 261-273.

Hamrick, J. M., 1992: A three-dimensional environmental fluid dynamics computer code: Theoretical and computational aspects. The College of William and Mary, Virginia Institute of Marine Science, Special Report 317, 63 pp.

Hamrick, J. M., and T. S. Wu, 1997: Computational design and optimization of the EFDC/HEM3D surface water hydrodynamic and eutrophication models. *Next Generation Environmental Models* and *Computational Methods.* G. Delich and M. F. Wheeler, Eds., Society of Industrial and Applied Mathematics, Philadelphia, 143-156.

Hayter, E. J., and A. J. Mehta, 1983: Modeling fine sediment transport in estuaries. Report EPA-600/3-83-045, U.S. Environmental Protection Agency. Athens, GA>

Hayter, E.J., M. Bergs, R. Gu, S. McCutcheon, S. J. Smith, and H. J. Whiteley, 1998: HSCTM-2D, a finite element model for depth-averaged hydrodynamics, sediment and contaminant transport. Technical Report, U. S. EPA Environmental Research Laboratory, Athens, GA.

Hwang, K.-N, and A. J. Mehta, 1989: Fine sediment erodibility in Lake Okeechobee. Coastal and Oeanographic Enginnering Dept., University of Florida, Report UFL/COEL-89/019, Gainsville, FL.

Laursen, E., 1958: The total sediment load of streams *J. Hyd. Div. ASCE*, **84**, 1-36.

Letter, J. V., L. C. Roig, B. P. Donnell, Wa. A. Thomas, W. H. McAnally, and S. A. Adamec, 1998: A user's manual for SED2D-WES, a generalized computer program for two-dimensional, vertically averaged sediment transport. Version 4.3 Beta Draft Instructional Report, U. S. Army Corps of Engrs., Wtrwy. Exper. Sta., Vicksburg, MS.

Le Normant, C., E. Peltier, and C. Teisson, 1998: Three dimensional modelling of cohesive sediment in estuaries. in Physics of Estuaries and Coastal Seas, (J. Dronkers and M. Scheffers, Eds.), Balkema, Rotterdam, pp 65-71.

Lick, W., and J. Lick, 1988: Aggregation and disaggregation of fine-grained lake sediments. *J Great Lakes Res.*, **14**, 514-523.

Mehta, A. J., E. J. Hayter, W. R. Parker, R. B. Krone, A. M. Teeter, 1989: Cohesive sediment transport. I: Process description. *J. Hyd. Engrg.*, **115**, 1076-1093.

Mehta, A. J., T. M. Parchure, J. G. Dixit, and R. Ariathurai, 1982: Resuspension potential of deposited cohesive sediment beds, in *Estuarine Comparisons*, V. S. Kennedy, Ed., Academic Press, New York, 348-362.

Mehta, A. J., and F. Jiang, 1990: Some field observations on bottom mud motion due to waves. Coastal and Oeanographic Enginnering Dept., University of Florida, Gainsville, FL.

Mellor, G. L., and T. Yamada, 1982: Development of a turbulence closure model for geophysical fluid problems. *Rev. Geophys. Space Phys.*, **20**, 851-875.

Meyer-Peter, E. and R. Muller, 1948: Formulas for bed-load transport. Proc. Int. Assoc. Hydr. Struct. Res., Report of Second Meeting, Stockholm, 39-64.

Middleton, G. V., and P. R. Wilcock, 1994: Mechanics in the Earth and Environmental Sciences. Cambridge University Press, Cambridge, UK.

Nielsen, P., 1992: *Coastal bottom boundary layers and sediment transport*, World Scientific, Singapore.

Park, K., A. Y. Kuo, J. Shen, and J. M. Hamrick, 1995: A three-dimensional hydrodynamic-eutrophication model (HEM3D): description of water quality and sediment processes submodels. The College of William and Mary, Virginia Institute of Marine Science. Special Report 327, 113 pp.

Rahmeyer, W. J., 1999: Lecture notes for CEE5560/6560: Sedimentation Engineering, Dept. of Civil and Environmental Engineering, Utah State University, Logan, Utah.

Raukivi, A. J., 1990: *Loose boundary hydraulics*. 3rd Ed. Pergamon, New York, NY.

Ried, I., and L. E. Frostick, 1994: Fluvial sediment transport and deposition. in *Sediment Transport and Depositional Processes*, K. Pye, ed., Blackwell, Oxford, UK, 89-155.

Shrestha, P. A., and G. T. Orlob, 1996: Multiphase distribution of cohesive sediments and heavy metals in estuarine systems. *J. Environ. Engrg.*, **122**, 730-740.

Smagorinsky, J., 1963: General circulation experiments with the primative equations, Part I: the basic experiment. *Mon. Wea. Rev.*, **91**, 99-152.

Smith, J. D., and S. R. McLean , 1977: Spatially averaged flow over a wavy bed. *J. Geophys. Res.*, **82**, 1735-1746.

Smolarkiewicz, P. K., and T. L. Clark, 1986: The multidimensional positive definite advection transport algorithm: further development and applications. *J. Comp. Phys.*, **67**, 396-438.

Smolarkiewicz, P. K., and W. W. Grabowski, 1990: The multidimensional positive definite advection transport algorithm: nonoscillatory option. *J. Comp. Phys.*, **86**, 355-375.

Spasojevic, M., and F. M. Holly, 1994: Three-dimensional numerical simulation of mobile-bed hydrodynamics. Contract Report HL-94-2, US Army Engineer Waterways Experiment Station, Vicksburg, MS.

Stark, T. D., 1996: Program documentation and users guide: PSDDF primary consolidation, secondary compression, and desiccation of dredge fill. Instructional Report EL-96-xx, US Army Engineer Waterways Experiment Station, Vicksburg, MS.

Suzuki, K., H. Yamamoto, and A. Kadota, 1998: Mechanism of bed load fluctuations of sand-gravel mixture in a steep slope channel, Proc. of the 11th congress of APD IAHR, Yogyakarta, pp.679-688.

Tsai, C. H., S. Iacobellis, and W. Lick, 1987: Floccualtion fo fine-grained lake sediments due to a uniform shear stress. *J Great Lakes Res.*, **13**, 135-146.

van Niekerk, A., K. R. Vogel, R. L Slingerland, and J. S. Bridge, 1992: Routing of heterogeneous sedimetns over movable bed: Model development. *J. Hyd. Engrg.*, **118**, 246-262.

Van Rijin, L. C., 1984a: Sediment transport, Part I: Bed load transport. *J. Hyd. Engrg.*, **110**, 1431-1455.

Van Rijin, L. C., 1984b: Sediment transport, Part II: Suspended load transport. *J. Hyd. Engrg.*, **110**, 1613-1641.

Villaret, C., and M. Paulic, 1986: Experiments on the erosion of deposited and placed cohesive sediments in an annular flume and a rocking flume. Coastal and Oeanographic Enginnering Dept., University of Florida, Report UFL/COEL-86/007, Gainsville, FL.

Ziegler, C. K., and B. Nesbit, 1994: Fine-grained sediment transport in Pawtuxet River, Rhode Island. *J. Hyd. Engrg.*, **120**, 561-576.

Ziegler, C. K., and B. Nesbit, 1995: Long-term simulation of fine-grained sediment transport in large reservoir. *J. Hyd. Engrg.*, **121**, 773-781.

Yang, C. T., 1973: Incipient motion and sediment transport. *J. Hyd. Div. ASCE*, **99**, 1679-1704.

Yang, C. T., 1984: Unit stream power equation for gravel. *J. Hyd. Engrg.*, **110**, 1783-1797.

Yang, C. T., and A. Molinas, 1982: Sediment transport and unit streams power function. *J. Hyd. Div. ASCE*, **108**, 774-793.

9. Figures

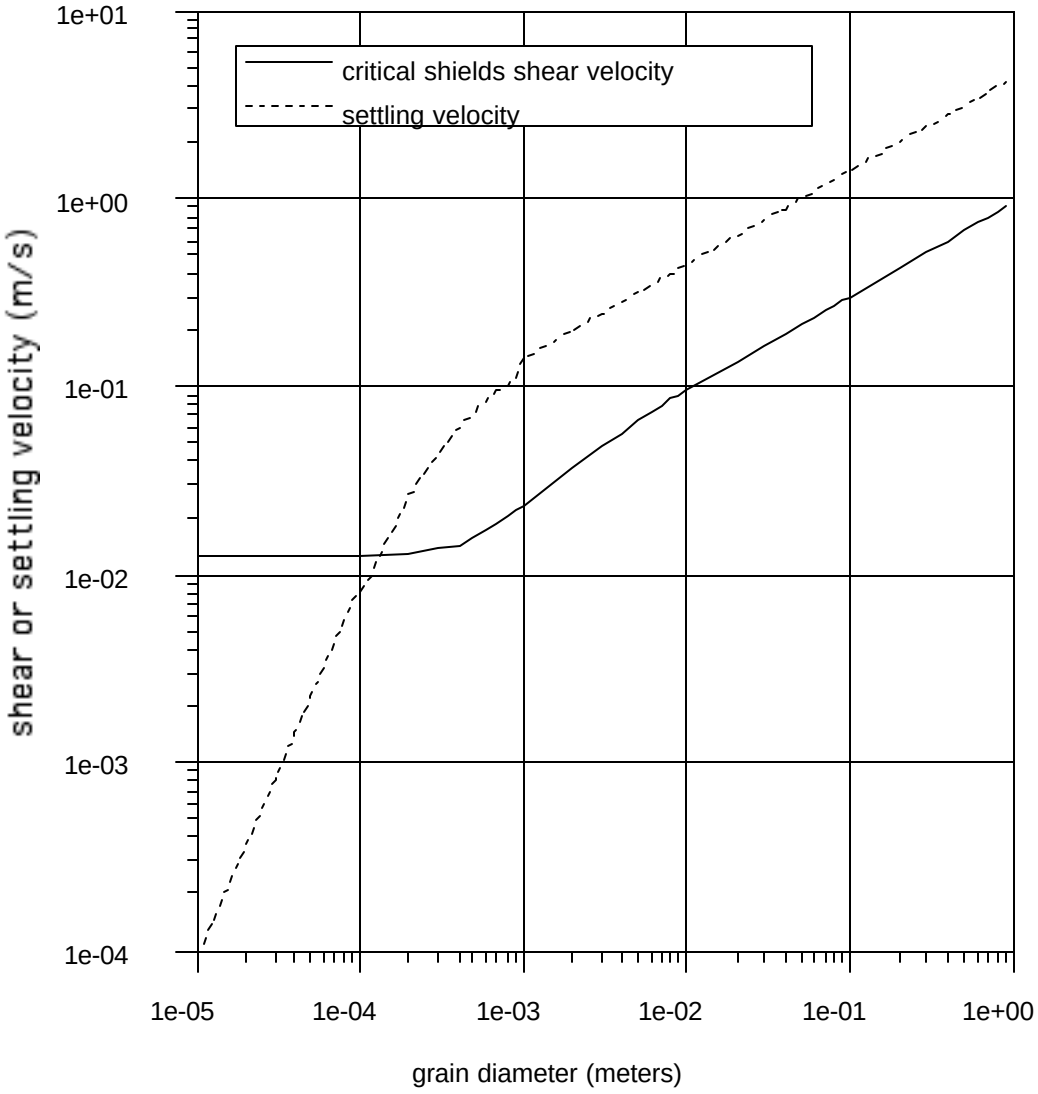

Figure 1. Critical Shield's shear velocity and settling velocity as a function of sediment grain size.